Experimental studies of a damaged ship section in forced heave motion

M.A. Siddiqui[1*], M. Greco[1,2], C. Lugni[1,2], O.M. Faltinsen[1]
1 *Centre for Autonomous Marine Operations and Systems (AMOS), Department of Marine Technology, NTNU, Otto Nielsens Vei 10, 7491, Trondheim, Norway*
2 *CNR-INM, Institute of Marine Engineering, Via di Vallerano 139, 00128 Roma, Italy*

mohd.a.siddiqui@ntnu.no

Abstract

This work documents a detailed series of experiments performed in a wave flume on a thin walled prismatic hull form. The model consists of a rectangular opening located on the side. The length of the model is slightly smaller than the flume breadth to achieve two-dimensional (2D) behavior in the experiments. Forced oscillatory heave tests in calm water have been carried out by varying the model-motion parameters and examining both intact and damaged conditions. Video recordings, measurements of the wave elevation inside the damaged compartment and of the force on the model were performed in all the experiments. The effect of damage opening in the model on hydrodynamic loads is examined by comparing with an intact section. A theoretical analysis is used to explain the behavior of added mass and damping coefficients in heave for a 2D damaged section. The presented results demonstrate occurrence of sloshing and piston mode resonances in the tests and their influence on the hydrodynamics loads of a damaged ship. Detailed physical investigations are presented at these resonance frequencies for the damaged section. Effect of filling level in the damage compartment, damage-opening length and air compressibility in the airtight compartment is examined. Nonlinear effects are documented and appear dominant, especially, for lowest filling level where we have shallow-water depth conditions in the damaged compartment. Resonance phenomena that can lead to significant local loads are identified for the shallow water condition. Air compressibility in the airtight compartment and floodwater act as a coupled system and influence inflow/outflow of floodwater in the compartment. It has a significant effect on local floodwater behavior in the damaged compartment.

Keywords: **Ship model experiments, Damaged ship hydrodynamics, Sloshing & Piston mode resonance**

Nomenclature

ζ_a	wave elevation amplitude inside damaged compartment
ζ^*	non-dimensional wave elevation amplitude inside damaged compartment
η_{3a}	amplitude of oscillation for forced heave motions
ω	angular frequency of forced oscillation in heave
ω^*	non-dimensional frequency
ω_{ns}	natural frequency for sloshing mode
ω_{np}	natural frequency for piston mode
ε	phase difference between heave displacement and force in heave

ρ density of water

γ Euler's constant

κ ratio of specific heats of air

A_r submerged area at equilibrium

A_{wp} area of waterplane for an intact section

A_{wpd} area of waterplane for a damaged section

A_{33} 3D added mass coefficient in heave

a_{33} 2D added mass coefficient in heave

a_{33}^* 2D non-dimensional added mass coefficient in heave

B breadth of model

B_c breadth of damaged compartment

B_{33} 3D hydrodynamic damping coefficient in heave

b_{33} 2D hydrodynamic damping coefficient in heave

b_{33}^* 2D non-dimensional hydrodynamic damping coefficient in heave

C_{33} restoring coefficient in heave

D depth of model

d length of side damage

d_T draft (submergence depth) for the model

F heave force

g acceleration due to gravity

h water depth/filling level inside the flooded compartment

h_c height of damaged compartment

h_d height of damage opening

i imaginary unit

k_0 wavenumber

L length of model

L_c length of damaged compartment

l_b length of baffle

M dry mass of model

M_w floodwater mass in stationary condition

p_a atmospheric pressure

T time period of heave motion

T_n natural period of sloshing / piston mode resonance

1 Introduction

Flooding in ships is usually a result of damage caused by collision, grounding or violent interaction with severe sea environment. Estonia disaster (1994) is an example where the bow visor did not close properly due to a glitch in the closure mechanism. Slamming due to waves may have caused the visor to fall off leading to flooding, water accumulation, loss of stability and finally capsize with loss of around 800 lives. Costa Concordia (2012) is another example of a ship disaster. In this case, the ship capsized due to grounding. Dramatic capsizes like these have led to large number of studies on ship flooding consequences.

When a ship experiences a damage event, the behavior of the ship is substantially modified. Flooding occurs through the damaged opening, in general affecting the stability properties and in the worst case causing the ship to capsize. Loss of lives can be enormous depending on ship mission and features. Roll On/Roll Off (RO-RO) ferries have become very popular on shorter sea routes and transport a large number of people and vehicles. These ships have usually large deck areas and even small amount of floodwater can lead to instability due to free-surface effect. Therefore, they are more susceptible to capsize as compared to other vessels. Although the principle can apply to any ship in general. Most ships are designed keeping in mind damaged stability considerations and requirements for static conditions. However, it is important to understand the features of flooding dynamics and the influence of floodwater on the dynamic stability of a damaged vessel in waves.

Various numerical methods have been proposed to study the behavior of damaged ship sections. Spouge [1] presented one of the earliest works for simulation of a damaged ship. He simulated the capsizing of the RO-RO vessel ‘European Gateway’. He used a hydraulic orifice flow model to calculate the flow of fluid through a small orifice between two fluid chambers, and empirical equations to determine the center of gravity (CG) of the floodwater. Spanos and Papanikolau [2] used a lumped mass method to simulate floodwater dynamics. The surface of floodwater is assumed to be horizontal regardless of ship motions. The lumped mass model assumes that the floodwater is located at its CG and moves so to remain always parallel to the sea surface. This approach gives reasonable results when sloshing effect is not dominant. Jasionowski [3] used a 6 degree of freedom (DoF) ship model to study damaged ship motions. He used a hydraulic flow model to account for inflow/outflow of floodwater and a free mass model instead of a rigid lumped mass model. The free mass model means that the floodwater is decomposed into small masses over the entire flooded compartment. Ruponen [4] presented an iterative time-domain solver for the simulation of flooding in ships and validated it against experiments on a damaged barge model. Santos and Soares [5] used shallow-water equations to solve the problem of flooded water on decks with the assumption that the water height on flooded deck must be small compared to deck dimensions. Hybrid methods have become popular in recent years with increase of available computational power. Colicchio et al. [6] used a domain

decomposition strategy to study water on deck problem. The problem was split into two domains exchanging information at their common boundary. A 2D Boundary element method (BEM) was coupled with a single-phase Navier Stokes (NS) solver. Gao [7] used a hybrid method that combined a NS fluid dynamics solver with a potential seakeeping solver to study motions of a damaged ship in waves. More recently, Sadat-Hosseini et al. [8] performed 6-DoF CFD simulations for a damaged passenger ship in calm water and in beam-sea waves and demonstrated better predictions compared with potential-flow solvers. Hashimoto et al. [9] presented numerical simulations for flooding in damaged ships and validated them against experimental data for forced roll motions and flooding test of a Pure Car and Truck Carrier model. They used a hybrid model combining a potential-flow solver for the intact region of the ship and a Moving Particle Simulation for the damaged region.

Although the available models can properly predict most of the behavior, we still lack practical tools for design implementation. Due to the complex nature of the problem and highly nonlinear behavior of the floodwater and its coupling with ship motions, detailed investigations need to be performed. They will be useful to assess reliability of simplified approaches able to capture the parameters governing the problem of a damaged ship in waves.

Various authors have performed model tests on damaged ships. Korkut et al. [10] conducted an experimental study on 6 DOF motion response for a RO-RO ship model in intact and damaged conditions. Begovic et al. [11] examined motions of a frigate hull in intact and damaged conditions. Both of the aforementioned studies highlight the change in ship motions for intact and damaged condition in waves. Palazzi and de Kat [12] performed model tests on a damaged ship model taking into account the effect of air compressibility in an airtight damaged compartment. They compared the test with numerical results and showed good agreement. They modeled airflow using gas laws and flow through an orifice. They noted that air compressibility may cause extra roll damping and concluded that airflow effects must be taken into account during simulations. Air compressibility effects on motions of a damaged ship were also examined by Ruponen et al. [13] and Khaddaj-Mallat et al. [14]. The latter identified damage opening area, damage location and air compressibility in damaged compartment, as important factors for flooding. Lee et al. [15] conducted a series of experiments on a damaged ship to be used for validating a CFD code. Manderbecka et al. [16] conducted experiments on a box shaped barge. They presented results for transient flooding cases for different widths of damaged compartments. Domeh et al. [17] conducted experiments on a damaged ship to study the effect of permeability and arrangement of damaged compartments on the behavior of a flooded ship. They also examined the effect of orifice size on the flooding behavior. They concluded that compartment permeability and orifice size have a larger effect on heave and pitch motions when the vessel has a forward speed with respect to a stationary condition. Acanfora et al. [18] performed experiments on a damaged ferry hull in beam-sea waves and studied the importance of location of damage for the roll response.

Forced motion tests to calculate hydrodynamic coefficients of damaged ship models have also been performed by some authors. Cichowicz et al. [19] performed forced roll experiments on a body with a flooded compartment. The model was a cylindrical midship section of a RO-RO Passenger ferry (RO-PAX) and had an internal gyroscopic mechanism designed to produce periodic roll moment. Tests were conducted both in intact and damaged condition. They presented added mass and damping in roll for a flooded ship model and reported negative added mass at low frequencies. The authors argued that this might be caused by slightly underestimated restoring coefficient. Hashimoto et al. [9] also presented experimental results for a damaged ship model undergoing forced roll motions. Smith et al. [20] also performed a series of forced

experiments in heave on a damaged ship model. The damage location was at the keel and extended along the length of the keel. Experimental setup was similar to Vugts [21] and the hydrodynamic loads were expressed per unit length and made non-dimensional as 2D loads so that the experimental results can be interpreted as 2D results. Added mass and damping in heave for a flooded ship model section were presented. They show a clear change in behavior and in particular that the values for damaged condition are much higher for both added mass and damping coefficients in the region of low frequencies. Effect of air compressibility in the damaged compartment was also demonstrated.

The flooded water inside a damaged compartment can experience resonance conditions. In particular, both sloshing and piston mode resonance can be excited in practical cases. Sloshing is an internal flow problem associated with a liquid having a free surface in a closed tank. It has been studied in detail with regard to transportation problems, especially for example in Liquid Natural Gas (LNG) ships. Faltinsen and Timokha [22] studied sloshing in a tank with internal structures, screens and chamfers. They provided analytical solutions for 2D and 3D sloshing in rectangular and in cylindrical tanks. They also developed a nonlinear multimodal method to study nonlinear sloshing and demonstrated good comparison with experiments. Rognebakke and Faltinsen [23] described coupling of ship motions with sloshing in internal tanks both experimentally and theoretically. The effect of internal sloshing on sway and roll motions of a ship is utilized in the development of anti-roll tanks. Piston mode resonance is connected with an external flow with an opening and appears as a pumping in-and-out flow. Kristiansen and Faltinsen [24] studied piston mode resonance between a ship and a terminal. They implemented a nonlinear BEM method with a discrete vortex method to study the behavior numerically. They also conducted experiments to validate their numerical method. Kong and Faltinsen [25] studied numerically the importance of sloshing and piston mode resonance in a damaged ship. They documented good agreement of their numerical results with ITTC benchmark experiments and discussed the importance and effect of these resonances. The effect of piston mode and sloshing resonance on roll motions is documented in figure 2 of [25], where Kong and Faltinsen have matched their results with ITTC experiments. In figures 3-9, they have documented the effect of piston and sloshing mode resonance on the hydrodynamic added mass and damping coefficients in the six degrees of freedom. The effect on the hydrodynamic coefficients is large, especially for heave, roll and pitch motions. de Kat [26] studied numerically and experimentally the motions of a ship with a partially flooded tank. He presented the effect of filling ratios on the first natural mode of sloshing in a flooded compartment. He also demonstrated how flooding affects the roll natural period of the damaged ship. To our knowledge, no experimental studies available in literature focused on sloshing and piston mode resonance for a damaged ship section and their effect on damaged ship hydrodynamic loads. Excitation of resonance can be significant in some cases leading to large hydrodynamic loads, as shown in present studies.

Here, we examine the behavior of floodwater in a damaged ship section with focus on the occurrence and effect of sloshing and piston mode resonance. The work by Kong and Faltinsen [25] is taken as inspiration and the sloshing studies performed by de Kat [26] are extended with more in-depth analysis. The latter studied mainly the excitation of the first sloshing mode, in our case we also attempt to examine the effect of second sloshing mode and piston mode resonances. For our investigation, we selected a simplified damaged-ship scenario with the aim 1) to carry on a fundamental-type research that could provide insights on the involved physics of flooding and resonance behavior of floodwater, and 2) to have clean model tests for validation of numerical methods to be used for systematic investigations. In particular, we study forced heave motion of a flooded section in calm water and the influence of floodwater on the hydrodynamic coefficients. Lateral motions (sway or roll) also excite resonance in the floodwater. The fact that heave

motions excite similar resonance behavior may not a priori be expected. In addition, the amplification of the free surface and corresponding resonance modeshapes are easier to identify in case of forced heave motions. Thus, a simplified single DoF model in forced heave motion has been investigated in the present work. Chang [27] investigated survivability of RO-RO ships and reported that damage at the midship is more dangerous compared to damage in other parts of the ship in beam-sea conditions. He used a nonlinear strip-theory method and validated with experimental results. His conclusions are based on a parametric investigation in terms of damage location, vehicle deck division and damage freeboard. Khaddaj-Mallat et al. [14] also used a midsection hull model of a passenger ferry as used for our case but they had internal deck subdivisions. RO-RO ships have generally large unobstructed decks to accommodate large number of cars. In this perspective, a simple single decked compartment can help identifying local resonance phenomena for floodwater. Using these findings as guidance, present model is designed as a midship section with a large open deck similarly as for a RO-RO carrier. The location of the damage is chosen to be at the side of the ship consistently with beam-sea damage. Detailed analysis is done near the sloshing and piston mode frequencies. A simplified theoretical method is used to estimate these resonance frequencies. Air compressibility effects inside a damaged compartment and effect of size of damage opening are examined. The remaining of the paper is structured as follows. Section 2 describes the experimental setup and conditions used in the experimental analysis. It gives a detailed description of the model section used, as well as the layout of the equipment and wave probes inside the model. Section 3 presents simplified analysis for estimation of sloshing and piston mode frequencies for the damaged section. Section 4 provides the analysis performed on the data acquired from various equipment during the model tests. Possible error sources in the tests are also listed. Section 5 discusses the experimental results. Added mass and damping coefficients in heave and wave elevation amplitudes inside the flooded compartment are presented for the damaged section. Finally, conclusions and shortcomings from the present study are provided to benefit other researchers in this field.

2 Experimental set-up and test conditions

Here, an experimental study was carried out on a damaged ship cross-section in forced heave motions inside a small wave tank 15 m long, 0.58 m wide and with a water depth of 0.9 m at the Marine Technology Centre, NTNU. We use a setup similar to the one described by Vugts [21] in his experiments on prismatic hull forms. The width of the used model is very close but smaller than the width of the flume so to obtain predominantly 2D behavior. The wave flume has plexiglass walls, which together with the plexiglass on the model, allow a clear visualization of the water-body interactions. It is equipped in present tests with two parabolic beaches at both ends for absorption of body-generated waves.

2.1 The model

The model was made of aluminum plates, divinicell (compressed foam), wood and fiberglass on front side for viewing inside the damaged compartment. Prior to starting the experiments, the model mass was measured. A schematic view of the designed and actual models is shown in figure 1. The main dimensions of the model and of the internal compartment are described in table 1. The model length (L) and breadth (B) are in the transverse and longitudinal tank directions, respectively. The table also provides the intended scale ratio of the experiments.

Figure 1 (right) shows the layout of the internal compartment inside the model. The length d of the opening on the damage side is modified to study the effect of damage size on the floodwater behavior. The two

opening sizes, and the cases associated with them, are referred to as opening 1 (O1) and opening 2 (O2) in this text. Opening 1 extends along the whole length of the flooded compartment, i.e, d=L_c. Figure 2 shows the two opening configurations used in the experiments. The right side of the figure shows appendages (thin wooden plates) added at the damage opening to reduce the damage size, d=7/10 L_c. These appendages will cause more vortex shedding as compared to opening 1 and introduce three-dimensional flow features. Opening 2 also provides more restriction to inflow/outflow through the opening. Dimensions for the two damage openings are given in table 2.

2.2 Equipment description

Figure 3 provides a simplified sketch of the experimental set-up for forced heave motions in the (y,z) cross-sectional plane. For performing the forced heave motion tests, the model is rigged with a linear oscillator connected through a support mechanism. A supporting frame with two beams along the breadth is used at the top of the model. It has been suitably designed to get pure forced heave in the form of steady-state oscillatory motion $\eta_3 = \eta_{3a}\sin(\omega t)$, after an initial ramp function has died out. Here *t* is the time variable, $\omega = 2\pi / T$ is the angular frequency of oscillation and η_{3a} is the heave amplitude. Parabolic beaches are placed at both ends of the flume to absorb radiated waves. The length of the beaches is around 1.5 m. The top parts of the beaches are placed 2-3 mm below the water surface. Load cells were mounted on the oscillator to measure the force components in the y and z directions and. From the vertical force, the heave added mass and damping coefficients associated with forced-heave oscillations can be estimated. Three accelerometers (Acc1-3) were placed on the model as shown in figure 4 to measure heave acceleration and check the quality of the actual heave motion with respect to the prescribed forced motion. The motion of the free surface inside the compartment was recorded using a digital camera with a video frame rate of 60 fps. The frame quality varied for some videos but it was never lower than 640x480 pixels. Two capacitance-type twin wire wave probes were located inside the model at a distance 0.25B (WP1) and 0.75B (WP2) from the opening to measure the wave elevation inside the damaged compartment. The wire diameter for the wave probes is around 1 mm. Sampling frequency for all data recorded in the measurements was 200 Hz. The duration of each test varied between 120 and 180 seconds depending on the heave oscillation period T. In this way, each test lasted at least 60T in order to achieve steady-state conditions in the forces on the model and in the flow features.

2.3 Test description

In our tests, three oscillation amplitudes and ten to fifteen forcing periods have been investigated for the forced heave motion, assuming three different drafts for the ship cross-section model. There is a limit for the largest forced-heave amplitude that can be studied in the used experimental set-up. The amplitude should not cause an overload for the employed linear oscillator. For this reason, we ensured that the dynamic forces due to the oscillations in heave were within 75% of the maximum load capacity of the oscillator. Within this limit, the three selected heave amplitudes are small relative to the examined values of the body draft, i.e. they are expected to result in linear hydrodynamic loads for an intact section. We investigate importance of nonlinear effects induced by the presence of a damage and by the related flooding phenomena. The selected forcing periods correspond to full-scale values of 3.5 to 16.5 seconds. These lie within the operating range of sea-going vessels. Changing the draft of the model corresponds to change of the filling depth for the damaged compartment. Details for the filling depths examined here are given in table 3. The distribution of the examined frequencies is not uniform but distributed to have a refinement

near natural sloshing and piston mode frequency regions. The experimental test matrix is given in table 4. For two filling levels, the model was made airtight to study the effect of air compressibility in the damaged compartment on the hydrodynamic coefficients. Effect of changing the damage-opening length was also examined.

3 Natural frequencies of water motion in a damaged compartment

The water motion inside the compartment has natural frequencies. This follows by finding non-trivial flow solutions and corresponding natural frequencies when the body is not excited. If we assume potential flow of incompressible water and linearize the free-surface conditions, we are looking for solutions of the velocity potential φ that satisfy the combined free-surface boundary condition on the mean free surface

$$-\omega^2\varphi + g\frac{\partial\varphi}{\partial z} = 0 \tag{1}$$

together with the body boundary conditions and radiation condition for the piston mode problem. Here ω means the circular frequency of oscillation, g is acceleration of gravity and the vertical $z-$axis is positive upwards.

If we consider no flow through the opening, the problem determines the so-called sloshing frequencies. There are also piston (pumping) mode resonance frequencies associated with in/outflow through the opening. The phenomenon is well known in harbor resonances, see for example work by Miles and Munk [28]. Piston mode resonance is also well known from moonpool analysis (Molin [29] and Faltinsen et al. [30]). Such analyses consider that the interior and exterior flow regions are coupled just like the damaged compartment in our case.

When the compartment is forced to oscillate vertically and there is no opening, resonant sloshing cannot be excited according to linear theory (Faltinsen and Timokha [22]). However, if we have an opening to the exterior water, the resulting water motion through the opening due to vertical tank motion implies resonant water motion in the compartment near the sloshing and piston mode natural frequencies. We can make the analogy with having a tank with a wave maker at the damage opening. The sloshing/floodwater motion inside the compartment is itself of a nonlinear nature combined with nonlinear external forcing due to the opening. For a 2D rectangular tank, the natural frequency of sloshing mode *j* is given by

$$\omega_{nsj} = \sqrt{g\frac{\pi j}{B_c}\tanh(\frac{\pi j}{B_c}h)}$$

Table 5 shows the non-dimensional sloshing frequencies for the first, second and third sloshing modes i.e. *j*=1, 2 and 3. In our case, we consider sloshing along the compartment breadth as the dominant sloshing direction; however, at high frequencies sloshing occurred also along the compartment length. A case of 3D sloshing is discussed later for filling level 2.

Newman et al. [31] studied an external 2D flow problem concerning forced heave motion of a submerged rectangle close to the free surface (right plot of figure 5). They used matched-asymptotic expansions for the solution of the problem that coupled the flow above a semi-infinite rectangle, $d_T \to \infty$, with the flow in the outer region. The problem solved by Newman et al. [31] implies a wall like condition at y=0. This means that there is an analogy between this problem and the case of damaged compartment with filling

level 1 (see left plot of figure 5). This can be seen by modeling the effect of the compartment side wall with a mirroring so that there is zero normal velocity at the wall position (see center plot of figure 5). Therefore, the solution of the submerged rectangle by Newman et al. [31] can be used as basis to estimate the natural piston-mode frequencies for our compartment at this filling depth and is discussed next. The details of the derivation can be found in Newman et al. [31], only the expressions needed for calculations and analysis in our case are presented below.

The edges of the submerged top of the rectangle have coordinates $z=-h$ and $y=\pm b$. On top of the rectangle the velocity potential is

$\phi=\frac{\mathrm{v}_0}{K}+A\cos(k_0 y)$, where $K=k_0\tanh(k_0 h)=\frac{\omega^2}{g}$, v_0 is the amplitude of heave oscillation velocity, k_0 is the wavenumber, and h is the submergence depth. A time dependence $\exp(i\omega t)$ is assumed in the analysis with i as the complex unit. After using matching conditions Newman et al. [31] derived

$$A=-(\frac{\mathrm{v}_0}{K})\left\{\cos(k_0 b)+(2/\pi)(k_0 h)\sin(k_0 b)\left[\ln(4Kh/\pi)+\gamma-1+\pi i\right]\right\}^{-1} \quad (2)$$

Here γ is the Euler's constant. The undamped resonance frequencies, referred to as the piston mode frequencies in the present work because of associated large inflow/outflow at these frequencies, can therefore be given by solving

$$\left\{\cos(k_0 b)+(2/\pi)(k_0 h)\sin(k_0 b)\left[\ln(4Kh/\pi)+\gamma-1\right]\right\}=0 \quad (3)$$

The equation follows by considering the real part of the expression (2) with real v_0 and calculating when it goes to infinity. Eq. (3) is an implicit equation and we solve for $k_0 b$, which can then be used to compute the natural piston mode frequencies. Subsequently, the force on top of the rectangle can be estimated to give the 2D non-dimensional added mass a_{33} and damping b_{33} as

$$(b_{33}+ia_{33})_{d_T\to\infty}=\frac{-2i}{\pi Kb}(1-Kh)+\frac{2i\sin(k_0 b)}{\pi K k_0 b^2}\left\{\cos(k_0 b)+(2/\pi)(k_0 h)\sin(k_0 b)\left[\ln(4Kh/\pi)+\gamma-1+\pi i\right]\right\}^{-1} \quad (4)$$

Newman et al. [31] introduced a correction for calculating added mass and damping of finite draft submerged rectangles. In particular, for a draft $d_T=2b$, they found non-dimensional hydrodynamic coefficients as

$$(b_{33}+ia_{33})_{d_T=2b}=(b_{33}+ia_{33})_{d_T\to\infty}+(b_{33}+ia_{33})_{SP} \quad (5)$$

Here $(b_{33}+ia_{33})_{SP}$ is the added mass and damping for a surface-piercing rectangle having draft d_T as $\frac{d_T}{2b}=1+\frac{h}{2b}$, where h is submergence depth of the rectangle (see figure 5). If we substitute $d_T=2b$ with the draft for our experiments, this means

$$a_{33}^{damaged,semi-Infinite}=a_{33}^{damaged}-a_{33}^{Intact};\ b_{33}^{damaged,semi-Infinite}=b_{33}^{damaged}-b_{33}^{Intact} \quad (6)$$

In section 5, eq. (6) will be used to assess qualitatively the force measurements from the tests. In particular, the 2D non-dimensional hydrodynamic coefficients for a semi-infinite submerged rectangle from eq. (4) are compared with $a_{33}^{damaged,semi-Infinite}, b_{33}^{damaged,semi-Infinite}$. These are estimated as the difference between the 2D non-dimensional hydrodynamic coefficients for the damaged model ($a_{33}^{damaged}, b_{33}^{damaged}$) and those for the intact model ($a_{33}^{Intact}, b_{33}^{Intact}$). The latter are calculated as described in section 4.

For filling level 2 and 3, the inner and outer water surface are not directly joined to each other but are vertically separated by the left side wall plate of the ship model. If we approximate the piston-mode condition at the opening as $\varphi = 0$ (see left plot of figure 6), which corresponds to zero vertical velocity, then this can be modeled by mirroring the damaged compartment about z-axis (see right plot of figure 6). This means that the natural piston-mode frequencies for the damaged compartment at these filling depths can be estimated examining a closed tank with double size of the damaged tank and with a vertical baffle at the center as studied by Faltinsen and Timokha [22]. Piston mode shapes calculated from Newman et al. [31] (see right plot of figure 7) demonstrate that $\varphi = 0$ at the opening is a valid approximation, we do not get exactly $\varphi = 0$ but close to zero value at the opening. Following the solution from Faltinsen and Timokha [22], the effect of the baffle on the natural eigenvalues of the compartment plus its mirror image is given by

$$\frac{\omega_n^{'2}}{\omega_n^2} = 1 - \frac{\pi g \frac{\partial \varphi_n}{\partial x}^2 l_b^2}{2\omega_n^2 \int\limits_{\Sigma_0 + \Sigma_{0M}} \varphi_n^2 ds} \tag{7}$$

where $\omega_n^{'}$ is the modified natural frequency due to presence of vertical baffle, ω_n is the natural frequency calculated from eq. (3), φ_n is the velocity potential for a tank plus its mirror image, Σ_0, Σ_{0M} is the mean free surface in the tank and its mirror image respectively and l_b is the submerged length of the baffle. The modes with zero velocity potential at the center plane of the fictitious tank are considered. The resonance periods for piston mode at all filling levels are shown in table 6. We see that the effect of a baffle on natural frequencies is small and is limited to a difference of 2%.

We must emphasize that Newman et al. [31] assumed an infinite depth condition for the outer region. In our case, this may be valid for higher frequencies but at smaller frequencies finite depth effects are non-negligible and thus we should take the resonance frequencies calculated in table 6 as an approximation for the present problem. It should be mentioned that sloshing resonance would not cause a change in vertical heave force because the mode shapes are such that the integrated dynamic pressure at the bottom of a clean tank would be zero. For the piston mode resonance, considerable vertical force occurs, especially for the first mode. This is because the asymmetry of the modes about the middle of the compartment leads to a non-zero vertical force in the tank (figure 7).

4 Data Analysis

Raw time histories of signals from the experiments contain data at the input frequency as well as some high-frequency content with small amplitudes. The raw signals from the instruments were low-pass filtered

to remove frequencies above 10 Hz. This removes all the high-frequency content, above the fifth natural sloshing mode. The Butterworth filter used does not cause any significant phase shift or reduction in amplitude of the signal at the forcing frequency. Figure 8 shows power density spectrum from Fast Fourier transform (FFT) of heave force measurements for two filling levels at a forcing frequency of 1.25 Hz. We see that the signal has a major peak at the input frequency, i.e. 1.25 Hz in this case. Nonlinear behavior is evident, as can be seen from the presence of small peaks at super harmonics, i.e. $2\omega, 3\omega, 4\omega....$. For filling level 1, we have the most significant nonlinear behavior with amplitudes at higher harmonics having values around 10% of the main harmonic amplitude. For filling level 2, it is a bit smaller, usually less than 5% of the first harmonic amplitude. Some high frequency content is seen around 12-20 Hz, this is noise related to the instrument and is present for all cases and frequencies. Similarly, for all cases, FFTs are performed on time histories of all measured quantities. The amplitude and phase of the signals are then calculated using the values at the forcing frequency.

For forced heave motions of intact section, in steady state conditions, the force part *F* oscillating with forcing frequency and measured by the load cells in the z direction, according to linear theory can be decomposed as follows

$$F = (m + A_{33}^{\ Intact})\ddot{\eta}_3 + B_{33}^{\ Intact}\dot{\eta}_3 + C_{33}^{\ Intact}\eta_3 \tag{8}$$

Here, *m* is the total mass of the oscillating system (see discussion below), $A_{33}^{\ Intact}$ and $B_{33}^{\ Intact}$ are, respectively, the linear frequency dependent hydrodynamic added mass and wave radiation damping coefficients in heave , $C_{33}^{\ Intact}$ is the restoring coefficient in heave. In the intact condition, $C_{33}^{\ Intact} = \rho g A_{wp}$, where $A_{wp} = LB$ is the intact waterplane area.

From this decomposition, in general *F* can be written as, $F = F_a \sin(\omega t + \varepsilon)$, where ε is the phase relative to forced heave motion. Substituting η_3 and *F* in eq. (8), gives

$$A_{33}^{\ Intact} = \frac{C_{33}^{\ Intact} - \frac{F_a}{\eta_{3a}}\cos(\varepsilon)}{\omega^2} - m \ \ ; B_{33}^{\ Intact} = \frac{F_a \sin(\varepsilon)}{\eta_{3a}\omega} \tag{9}$$

Assuming that strip theory is valid, for the intact section, the 2D added mass and damping is calculated as $a_{33}^{\ Intact} = \frac{A_{33}^{\ Intact}}{L}; b_{33}^{\ Intact} = \frac{B_{33}^{\ Intact}}{L}$, respectively.

For the damaged section in our case, with intact parts on the ends (figure 8), the force *F* measured by the load cells in the z direction can be decomposed into intact force from the end regions and force due to damage region in the middle, i.e.

$$F = \left[(m^{Intact} + A_{33}^{\ Intact})\ddot{\eta}_3 + B_{33}^{\ Intact}\dot{\eta}_3 + C_{33}\,\eta_3\right] + \left[(m^{damaged} + A_{33}^{\ damaged})\ddot{\eta}_3 + B_{33}^{\ damaged}\dot{\eta}_3\right] \tag{10}$$

Here, $C_{33} = \rho g A_{wpd}$, where $A_{wpd} = A_{wp} - B_c L_c$ is the end intact sections waterplane area.

Eq. (10) can be further re-written as

$$F = m\ddot{\eta}_3 + \left[A_{33}{}^{Intact}\ddot{\eta}_3 + B_{33}{}^{Intact}\dot{\eta}_3 + C_{33}\,\eta_3 \right] + \left[A_{33}{}^{damaged}\ddot{\eta}_3 + B_{33}{}^{damaged}\dot{\eta}_3 \right] \tag{11}$$

$m = m^{Intact} + m^{damaged}$. Following Smith et al. [14], *m* includes the dry mass of model and the equilibrium weight of floodwater inside the damaged compartment. We can calculate added mass and damping for the damaged section with intact ends as done above for an intact model in eq. (9) as

$$A_{33}{}^{measured} = \frac{C_{33} - \frac{F_a}{\eta_{3a}}\cos(\varepsilon)}{\omega^2} - m \quad ; B_{33}{}^{measured} = \frac{F_a \sin(\varepsilon)}{\eta_{3a}\omega} \tag{12}$$

where $A_{33}^{measured} = A_{33}^{Intact} + A_{33}^{damaged}$ $\qquad$ $B_{33}^{measured} = B_{33}^{Intact} + B_{33}^{damaged}$

Assuming that strip theory is valid, for the intact section at the ends,

$$A_{33}^{Intact} = a_{33}{}^{Intact}(L-d)\ , B_{33}^{Intact} = b_{33}{}^{Intact}(L-d) \tag{13}$$

The $A_{33}^{measured}$ and $B_{33}^{measured}$ values have some 3D effects due to intact regions at the ends. To get 2D added mass and damping for a completely damaged section (for example, green cross-section in figure 9) we must subtract the intact values for end regions given by eq. (13) and divide by the damage length as follows

$$a_{33}{}^{damaged} = \frac{A_{33}^{measured} - a_{33}{}^{Intact}(L-d)}{d}; b_{33}{}^{damaged} = \frac{B_{33}^{measured} - b_{33}{}^{Intact}(L-d)}{d} \tag{14}$$

where $a_{33}{}^{damaged}, b_{33}{}^{damaged}$ are the added mass and damping for a 2D damaged section, and L, d are length of the model and length of damage opening. Model tests for the intact section were performed for fewer frequencies as compared to the damaged section. The values for the intact section to be used in eq. (14) are interpolated for the missing frequencies from the experimental data for filling level 1 and 2. Unfortunately, intact tests were not performed for filling level 3 and therefore, we use experimental values of 2D added mass and damping from interpolated Vugts [21] data. The 2D hydrodynamic coefficients from eq. (14) are examined in detail in section 5 for the cases studied in present experiments. Resonance conditions will be discussed with reference to the sloshing and piston mode natural frequencies provided in table 5.

For an airtight damaged compartment, restoring coefficient used for the section needs to be given special attention. Restoring coefficients are associated with dynamic change in vertical force due to the influence of heave motion on hydrostatic loads. When we examine the air cushion, the pressure can be considered spatially constant and same as the pressure at the air-water interface. This implies that due to the high air stiffness, the floodwater almost acts as a solid mass oscillating with the damaged section. The consequence is a resulting restoring coefficient as if the section was intact and, therefore, for a damaged airtight section we use $C_{33}^{damaged,airtight} = C_{33}^{Intact}$.

4.1 Error Sources

Main error sources in the model tests are:

- Meniscus effect caused by surface tension in the steel wire wave probes. Faltinsen and Timokha [22] mention a bias error less than the diameter (1 mm) of the steel wire. For smaller amplitude of oscillation, 3 mm in our case, sometimes the wave elevation may be too small for some cases and thus within the error range.
- Three-dimensional flow effects are present and observed at higher frequencies because the transverse sloshing mode in the compartment may also be excited. 3D effects can also be present due to the small gap between glass walls of the flume and the model. However, in most cases these gap forces are negligible compared to the hydrodynamic heave force on the model (Kristiansen and Faltinsen [24]).
- Wave reflection from the beaches can be a source of error, using the group velocity relation we estimate that reflection can occur as soon as after 5 cycles for smaller frequencies. The actual wave reflection has not been measured. Ouellet and Datta [32] mention that a reflection of 10% is present even for well designed beaches. They mentioned that for wavelengths larger than 0.75 the length of a wave beach, it is nearly impossible to attain a reflection less than 10% from the beach. The latter corresponds to non-dimensional frequencies less than around 0.67 for our tests.
- Errors may be present due to some nonlinearity in the calibration factor of instruments. Usually, a small drift occurs in the signal over time and therefore, calibration of the instruments should be checked regularly.
- An error source is also the heave actuator, in the forced motion tests. In some cases, it did not attain the desired forced heave amplitude, ranging from 90-95% of the input heave amplitude. It is strictly not an error source since we know the measured amplitude from the test and have used that in the calculations. It is listed here though as the control system did not perform as expected. It is to be noted that the forced heave amplitude still reached steady state easily for each experimental test.

Error quantification for the instruments used in the tests is provided in table 7. Repeatability of the experiments is described at the end of section 5.

5 Results and Discussion

In this section, we present results for forced heave motions for the intact and damaged model section. The results are documented in terms of wave elevation amplitude inside the damaged compartment, added mass and damping coefficients in heave described in section 4 and examining the influence of filling depth inside the damaged compartment, of the opening size, and of the airtightness in the damaged compartment. The force measured in the horizontal direction is small and, therefore, we concentrate on the vertical hydrodynamic loads in the discussed results. Special attention is given to the occurrence of resonance phenomena for the liquid inside the damaged compartment and to the consequences for the hydrodynamic loads. Sloshing and piston mode resonance scenarios are presented using images from the tests with the green bold lines representing the 2D internal free surface outline inside the compartment. For the plots presented in this section, the vertical dashed lines correspond to the non-dimensional linear natural frequencies for sloshing and piston modes reported in table 5 and 6. All results in this section are made non-dimensional as follows:

$$\omega^* = \omega\sqrt{\frac{B}{2g}}\ ,\zeta^* = \frac{\zeta_a}{\eta_{3a}};\ a_{33}{}^* = \frac{a_{33}}{\rho A_r},\ b_{33}{}^* = \frac{b_{33}}{\rho A_r}\sqrt{\frac{B}{2g}}$$

where all symbols are as described before and $A_r = Bd_T$ is the submerged cross-sectional area of the model both for intact and damaged sections, and d_T is the submergence draft.

In calculation of added mass, damping coefficients and wave probe RAOs, we use the linear forcing frequency component from the FFT analysis of heave force and wave probe data. Therefore, presented results in this section are to be interpreted as linear added mass, damping, and wave elevation RAOs. Figure 10 shows 2nd and 3rd order force amplitudes associated with frequencies 2ω and 3ω divided by the force associated with the main forcing frequency ω from the experiments at filling level 1 and 2. We can see higher nonlinear behavior for filling level 1 as expected because of shallow-depth condition. For both filling levels, the nonlinear behavior is limited to less than 10% for the force values. The nonlinear behavior is more pronounced for local flow features as compared with the heave force, for example steep nonlinear waves for filling level 1 inside the damaged compartment.

5.1 Intact Condition

To quantify the influence of the damaged compartment on the hydrodynamic coefficients in heave, the model section was also tested as intact section in forced heave motions. A very thin wooden plate was used to cover the damage opening shown in figure 1 of the present model and sealed watertight. Figure 11 shows added mass and damping coefficients in heave from the present experiments for the two waterline conditions described in table 3. Within the examined frequency range, the results indicate a limited effect of the non-dimensional frequency on the dimensionless added mass, while the damping coefficient is larger for lower frequencies. We observe higher values for smaller drafts. This is a consequence of the way we non-dimensionalize the results.

5.2 Damaged Condition

Forced heave motions are performed on the model with opening exposed to external water in various configurations as described in section 2. We discuss the results in terms of linear added mass and damping coefficients in heave in this work. As mentioned earlier, Faltinsen and Timokha [22] mention that linear theory cannot predict sloshing excited by heave motion for liquid inside an intact section. In our case, as argued earlier, the opening acts as a wave maker. This can excite sloshing and piston mode resonance. However, the effect on heave added mass and damping depends on the symmetry properties of the mode shapes about the centre plane for sloshing and piston mode resonance. Figure 12 shows the model at different filling levels.

5.2.2 Influence of filling depths inside damaged compartment

Filling level 1: If the forcing frequency is in the vicinity of the lowest natural sloshing frequency, Faltinsen and Timokha [22] identify a shallow-depth condition for sloshing in a closed tank if $h/l<<0.1$, where h is the water depth in the tank and l is the tank breadth. In our case $h/B_c=0.03/0.5=0.06<<0.1$, therefore we have a shallow water condition for the floodwater inside the damaged compartment for our considered forcing frequencies. The wave systems in shallow water differ from those in higher filling depths for closed tanks. They were first described by Olsen and Johnson [33] and experimentally studied by Bouscasse et al. [34] for a closed rectangular tank under harmonic forced oscillations in sway. These wave systems are found in the vicinity of the lowest sloshing frequency. In particular, Olsen and Johnson [33] classified four wave systems, in terms of the lowest sloshing frequency ω_{ns1}. Wave system I ($\omega/\omega_{ns1}=0.645$), with

standing waves, mainly occurs for smaller frequencies and is associated with small elevation inside the compartment. Wave system II ($\omega/\omega_{ns1}=0.8$), with progressive waves travelling back and forth without breaking, involves water that moves towards the compartment wall and is reflected back with almost the same speed. Wave system III ($\omega/\omega_{ns1}=1$), with progressive breaking waves similar to wave system II but with breaking occurring at or near the tank wall and wave system IV ($\omega/\omega_{ns1}=1$), with hydraulic jumps travelling back and forth inside the compartment. Wave systems III and IV occur at the same forcing frequency depending on the ratio of the forcing amplitude and tank breadth. Wave system IV occurs for higher forcing amplitudes. Bouscasse et al. [34] reproduced typical free surface configurations as classified by Olsen and Johnson [33]. They also highlighted nonlinear effects associated with shallow water sloshing in forced sway motions. It is interesting to note that forced heave motions on a damaged section also generate similar phenomena as classified by Olsen and Johnson [33] near the sloshing frequencies in table 5. Piston mode resonance is also observed near the frequencies documented in table 6. An important observation is the presence of travelling waves in the compartment at certain frequencies in addition to the standing waves observed for sloshing resonance frequencies. These cases occur near the piston mode resonance.

Figure 13 shows wave RAOs at WP1 and WP2 inside the damaged compartment for filling level 1 (see left plot of figure 12). Figures 12-16 provide snapshots of the various wave systems occurring inside the damaged compartment for the shallow-water conditions examined in the present experiments. Figure 13 shows peaks in wave amplitude inside the compartment near $\omega^* = 0.73$ and $\omega^* = 1.4$ with a magnification of around 1.2 to 1.8 times the forced heave amplitude. WP2, which is close to the undamaged wall, has higher values at lower frequencies. The floodwater rises slowly inside the compartment along the wall and accumulates near the wall. After reflection from the wall, as the water reaches WP1, which is close to the opening, it decays in magnitude because floodwater partially goes out of the compartment due to conservation of fluid mass, so we get smaller values. At higher frequencies, the waves are reflected very quickly from the wall and do not have time to decay much until they reach WP1. In the meanwhile, more water enters through the opening. As a result, the two waves meet closer (giving large amplitudes) to WP1 than to WP2, resulting in a larger elevation for WP1 with respect to WP2 at higher frequencies. In summary, at low frequencies, the behavior inside the damaged compartment is dominated by external water and its in/out flow through the opening, whereas at higher frequencies the waves inside dominate the local behavior and the in/out flow through the opening is more limited. We observe similar behavior as Olsen and Johnson [33] but since they have described results for forced sway motions and we observe scenarios for forced heave motions, we do not expect the frequencies of the wave systems to be similar. Near the first sloshing resonance, i.e at $\omega^* = 0.55$, standing waves take place in the compartment (figure 14), similar to wave system I identified by Olsen and Johnson [33]. For higher frequencies, we get nonlinear progressive non-breaking waves (figures 15 and 16), similar to wave system II identified by Olsen and Johnson [33]. At $\omega^* = 1$, the flow inside the compartment resembles the second natural mode of sloshing with high wave steepness. This non-dimensional frequency is close to the calculated value of $\omega^* = 1.06$ (see table 5). Whereas at $\omega^* = 1.43$, a higher order mode is observed. In some cases, the waves impact the undamaged wall with splash up leading to water spray (figure 17). At the second piston mode resonance and highest forcing amplitude, scenario similar to wave system IV identified by Olsen and Johnson [33] is documented in figure 18. A large water mass rises along the compartment wall and gradually the hump travels back in the compartment towards the opening. We do not observe a hydraulic jump. The wave amplitudes inside

the compartment for the three forcing amplitudes are nonlinear as expected at this filling level. In addition, the waves generated at the smallest forcing amplitude are smaller and this may lead to larger measurement error from the wave probes in this case.

At certain frequencies and highest excitation amplitude $\eta_{3a} = 7\text{mm}$, breaking waves also occur in the middle of the tank as observed by Bouscasse et al. [34]. We see a similar behavior at $\omega^* = 1.25$ and for the highest forcing amplitude, i.e., $\eta_{3a} = 7\text{mm}$, as shown in figure 19, where part of the progressive wave is reflected from the wall and meets the incoming wave from the opening. This causes a secondary splash near the middle region that depends on the inflow. Such phenomena could cause high loading on an already damaged structure, in particular when the breaking happens near an interior structure. To investigate the quantitative danger, one should estimate the local loads induced on the compartment. This has not been done here, as it would require a dedicated setup and suitable pressure sensors possibly facing dry-wet conditions.

Figure 20 presents the non-dimensional added mass and damping coefficients in heave for filling level 1 obtained from eq. (14). The values of added mass at small frequencies show large negative values and large deviation from intact condition at the same stationary draft. At higher frequencies, we do not observe peaks but much smaller values as compared to the intact section. This is because the restoring coefficient in damaged case is calculated using damaged waterplane area as defined in section 4. The in/outflow of water through the opening is limited at higher frequencies with floodwater effect mostly local and does not cause a large change in the force as compared to an intact section. Thus, due to smaller restoring coefficient we get a smaller added mass. At smaller frequencies, especially piston mode, large inflow/outflow causes large additional water mass to oscillate with the model. Large change in vertical force occurs, which, coupled with a smaller restoring coefficient, leads to a negative added mass. Damping also increases at frequencies around the first and second piston mode i.e. $\omega^* = 0.27$ and $\omega^* = 0.73$ as compared to the intact ship section. This is related to the wave systems inside the damaged compartment, which help in wave generation capability of the damaged section. The behavior at the three forcing amplitudes is similar for the added mass except at the smallest forcing amplitude, especially for smaller frequencies. The damping shows much more nonlinear behavior. This may be related to nonlinear wave generation due to the opening.

Figure 21 compares the 2D added mass and damping coefficients in heave for a damaged section as given by eq. (6) with Newman et al.'s [31] potential-flow values (eq. (4)). We see good agreement at higher frequencies. Newman et al. [31] assumed the outside region has an infinite depth. At smaller frequencies, finite depth effects become non-negligible as mentioned earlier and we see deviation from the theoretical values, for example for non-dimensional frequencies less than 0.6 the wavelength is 4 times as large as the water depth, therefore non-negligible finite depth effects must be present below this frequency. Overall, the trend is reasonably predicted with large negative added mass values near first piston mode resonance, peak in damping near the first piston mode and a much smaller peak near the second piston mode resonance. In our case, the non-dimensional resonance frequency for the first piston mode is around 0.27, which is much smaller than the frequencies studied in the experiments. Therefore, we see values going towards a peak but we do not observe a large peak as for Newman et al. [31]. Also, the peak near the second piston mode is very small for Newman's expression to be seen in the figure but can be observed for experimental values.

Filling level 2: Piston mode and sloshing resonance modes are also observed for this filling level. The occurrence of these resonance phenomena is documented by the wave elevation RAO at WP1 and WP2

inside the compartment shown in figure 22. We see a high peak near the first piston mode resonance; a pumping piston mode occurs with a large in/outflow through the compartment (figure 23). The values for WP2 are higher than WP1, this is also observed in the experimental images and occur because the antinode at the wall is close to WP2 but there is almost a node-like condition near WP1, as we would expect in case of piston mode. We also see a major peak at higher frequencies near the second piston mode frequency (figure 24). In this case, WP1 has higher values as compared to WP2. This is because the antinode is now much closer to WP1 as compared to WP2. We also observe the first sloshing mode from video analysis, as documented in figure 25. In this case, WP1 and WP2 record RAO values between 0.6-0.8 but without a large peak. This is because the antinodes for piston modes are much closer to the wave probe locations as compared to sloshing modes. Also, for the second sloshing mode (figure 26), the wave probes actually lie at the nodes and thus we see very small values, as shown in figure 20. The RAOs generally document a linear behavior except for the smallest forcing amplitude and for small frequencies.

At very high frequencies, we also observe a 3D behavior inside the compartment (figure 27). We see the first sloshing mode along the length L_c of the tank and a sloshing mode along the breadth B_c of the tank. However, the amplitude associated with the mode along the length is much smaller as compared to the mode along the breadth.

Figure 28 shows non-dimensional added mass and damping coefficients in heave for filling level 2. We have a sharp change in added mass values, i.e. negative to positive peak, near the first piston mode resonance frequency and this is due to a large amount of water entering and leaving the damaged compartment and thus a large vertical force occurring at this resonance frequency. Also, at the first piston mode resonance change in phase shift occurs, which coupled with large force lead to large negative and positive added mass values. Similar behavior for heave added mass is documented in numerical studies carried out by Kong et al. [25] and in the analysis presented in Newman et al. [31]. In the present case, near the first piston mode resonance, there can be change of almost 3 cm in the water level inside the compartment. It corresponds to a change of 6 kg, i.e. 30% of dry mass M of the model, inside the compartment. This can cause a large change in the vertical force. At higher frequencies, we observe smaller values of added mass when compared with an intact section. The damping shows two peaks, a larger peak at the first piston mode region and a minor peak near the second piston mode frequency. The damping values are much higher when compared to those of an intact ship with the same draft near the first piston mode resonance. As mentioned earlier, the opening acts as a wavemaker with large wave amplitudes occurring near piston mode resonance and, therefore, a large amount of energy is radiated at piston mode frequencies, especially at the first piston mode. The curves for the non-dimensional hydrodynamic coefficients for different forcing amplitudes are practically superimposed except near the first piston mode resonance and highest forcing amplitude. This may be a consequence of vortex shedding at the opening top edge, which can have higher effect for higher forcing amplitudes.

Figure 29 shows comparison between 2D added mass and damping coefficients in heave for a damaged section from eq. (6) and Newman et al.'s [31] potential-flow values (eq. (4)) for filling level 2. Similar to filling level 1, good agreement is observed for higher frequencies but deviation occurs at smaller frequencies, as discussed earlier, due to finite depth effects. The agreement is better at this filling level compared to filling level 1, may be because the nonlinearities are less strong. The values from Newman et al. [31] for added mass show a jump from large negative to positive values at first piston mode resonance. The same is captured very well in the experiments. The peak in damping near the first piston mode and a

small peak near the second piston mode are also similar to results by Newman et al. [31]. The smaller peak in damping at second piston mode for Newman et al. [31] expression is too small to be seen in the figure.

Filling level 3: The wave elevation RAOs for WP1 and WP2 inside the compartment at filling level 3 are shown in figure 30. We see a similar behavior as observed for filling level 2, with peaks near the piston mode resonance frequencies. Figure 31 shows non-dimensional added mass and damping coefficients for filling level 3. The non-dimensional added mass coefficient has similar trends as for filling level 2. The damping values are slightly smaller when compared with those for filling level 2. This is because damping decreases with increase in draft, as mentioned earlier for an intact section. In addition, at smaller frequencies, we observe more nonlinear behavior for this case as compared to filling level 2. This may be due to flow separation effects at the opening edge, which become larger for this filling depth.

5.2.3 Influence of air compressibility

If the compartment is airtight, it can cause significant changes in behavior of water inflow/outflow to the compartment and therefore in the hydrodynamic-load coefficients. This effect has been investigated experimentally by sealing all air exits and openings. The resulting air cushion is illustrated in figure 32. The static pressure in the air cushion is $p_0 = p_a + \rho g h_{S_{FI}}$, where p_a is atmospheric pressure and $h_{S_{FI}}$ is the vertical distance of the internal free surface S_{FI} below the external free surface. In our case, $h_{S_{FI}} = 0.$ It follows from continuity of air mass in the air cushion and adiabatic pressure-density relation that the pressure in the air cushion is

$p_{gas}(t) = p_0 \left[\frac{\Omega_0}{\Omega(t)} \right]^{\kappa}$ where Ω_0 is the air cushion volume at rest and κ is the ratio of specific heats for air. Let us consider small changes in the air cushion volume. This can be expressed as

$$\Delta\Omega = L_c \int_{S_{FI}} \zeta \, dy$$

Here L_c is the length of the air cushion in the transverse model tank direction. The integral is along the internal free surface S_{FI} in the ship cross-sectional plane. Furthermore, ζ is the relative internal vertical free-surface elevation, i.e. with respect to the air-water interface in static conditions. It follows by Taylor expansion that the dynamic change in the air cushion pressure $p_{gas} - p_0$ can be expressed as

$$\Delta p = -p_0 \kappa \frac{\Delta\Omega}{\Omega_0}$$

The free-surface condition at the internal free surface can be derived similarly as Malenica and Zalar [35] did by using Bernoulli's equation, continuity of pressure and vertical velocity at the internal free surface. Therefore, we get

$$\frac{\partial^2 \varphi}{\partial t^2} + g \frac{\partial \varphi}{\partial z} - \frac{\kappa p_0}{\rho \Omega_0} \frac{\partial \Delta\Omega}{\partial t} = 0 \qquad (15)$$

where φ is the velocity potential describing the water flow.

Making eq. (15) non-dimensional implies that, together with geometric similarity, both Froude-number $Fr = \frac{U}{\sqrt{Lg}}$ and Euler-number $Eu = \frac{p}{\rho U^2}$ must be similar in model and full scale. Here U is the characteristic flow velocity and L is the characteristic length for a system. For instance, for the intended scale ratio in our case of 1:40, we need to scale down ambient pressure in model scale by 1:40. Since cavitation must be avoided, there is an operational limit on how much the air pressure can be lowered in the experiments. When there are small vent holes, we must introduce a non-dimensional parameter characterizing the mass flux to and from the air cushion that should be the same in model and full-scale conditions. Since the mass density of air is smaller in depressurized conditions, it implies the cross-sectional area of the vent holes must be modified in model scale. Ruponen et al. [13] circumvented the scaling issue by studying air compressibility effects on a full-scale ship model.

The described dynamic air cushion model with uniform pressure has a natural frequency. It is similar to a mass-spring system where the air compressibility causes the spring effect and the mass comes from generalized added mass associated with water oscillations generated by the air cushion oscillations (Faltinsen and Timokha [22]). Assuming the air cushion acts as a piston, Faltinsen and Timokha [22] give a simplified formula for calculation of the natural frequency of the air cushion as $\sigma_{nc} = \frac{2\pi}{T_{nc}} = \sqrt{\frac{4\kappa p_0}{\pi a^*_{33c} \rho \Omega_0}}$

where $a^*_{33c} = \frac{a_{33c}}{\rho\pi(B_c^2/4)}$ is non-dimensional added mass and a_{33c} the added mass associated with water oscillations generated by the air cushion oscillations with a high frequency condition at the external free surface. If we consider the undamaged wall on the right as a symmetry plane for the flow and neglect the rest of the structure, we find that $a^*_{33c} = 1$. This leads to a natural period of air cushion oscillations at filling level 2 and 3 in the model scale as $T_{nc} \simeq 0.05$ s and $T_{nc} \simeq 0.06$ s, respectively. It is expected that accounting for the complete structure will lead to larger high-frequency added mass values. For instance, as a rough estimate assuming the compartment floor has infinite extent, gives $a^*_{33c} = 3.63$ and $a^*_{33c} = 2.96$ for filling level 2 and 3, respectively. This leads to upper limit of natural periods of air-cushion oscillations for filling level 2 and 3 as $T_{nc} \simeq 0.095$ s and $T_{nc} \simeq 0.1$ s, respectively. Since, our examined range of forcing periods is considerably higher than these natural periods, the air-cushion acts as a stiff spring. In full scale, following a similar analysis, we get a rough estimate of natural frequency of air-cushion oscillations in the range $3 \le T_{nc} \le 6$ s. This lies within operating range of sea-going vessels, but it must be noted that the assumptions used in the above analysis are valid for high frequency conditions. However, we get a reasonable estimate of the relative ratio between oscillation frequencies of air-cushion in model and full scale. This also demonstrates that scaling effect must be addressed going from model to full scale.

Eq. (15) shows that if $\int_{S_{FI}} \zeta \, dy = 0$ for all time instants, then the water flow is not affected by the air cavity. The latter is satisfied at sloshing resonance but, for instance, not for piston mode resonance. Generally speaking, airtight condition has important influence on the wave scenarios inside the damaged compartment. Figures 33 and 34 show the wave elevation RAOs inside the compartment for airtight and ventilated cases at two filling levels, respectively. The results demonstrate that piston mode resonance is almost completely absent for an airtight compartment (figure 35), while it is clearly observed for the ventilated compartment. As mentioned earlier, air cushion does not have effect on the sloshing resonance

in the compartment. We observe a clear peak at first sloshing resonances for filling level 2 and 3 in case of an airtight compartment similar to the ventilated compartment. In general, the free-surface elevation in airtight condition is lower than for the ventilated compartment. The reason is associated with the fact that forcing periods are clearly higher than the air cushion resonance period as demonstrated by earlier analysis. The air cushion acts then like a stiff spring and restrains the water elevation.

Figures 36 and 37 show the non-dimensional added mass and damping coefficients in heave for filling levels 2 and 3, respectively, in airtight and ventilated conditions. The damping values for an airtight damaged compartment are similar to intact condition, as shown for filling level 2 (figure 36). The damping values are much lower for the airtight cases as compared to ventilated damaged compartment, especially near the first and second piston mode resonance. Piston mode resonance is absent and a wall like condition occurs at the opening, leading to small in/outflow and, therefore, small wave radiation due to exchange of floodwater. This behavior is consistent for both filling levels. Sloshing resonance occurs and, therefore, the damping values for airtight and ventilated conditions are similar. The added mass coefficients for airtight condition do not show large negative values and have similar behavior as for the intact condition, with slightly higher values at smaller frequencies. This is again related to absence of piston mode resonance for a damaged airtight compartment. For the airtight compartment, the floodwater behaves almost as a solid mass oscillating with the model and the dynamic forces near piston mode frequencies are highly reduced. As described earlier, sloshing resonance does not cause change in added mass behavior and therefore, values for airtight and ventilated damaged compartments are similar at sloshing frequencies. We must emphasize that the restoring coefficient in the airtight case is much larger as compared to a ventilated damaged section.

5.2.4 Influence of damage opening breadth

The effect of opening size is examined using opening 1 and 2 scenarios as mentioned in section 2. Figures 38 and 39 show the wave amplitude RAOs inside the compartment for the two openings at filling levels 1 and 2, respectively. For filling level 1, WP1 has smaller values for opening 2 since the inflow is restricted to some extent and it is harder for the water to enter as compared to the larger opening. This effect is only observed for small frequencies because in this case it takes more time for inside wave systems to adjust to the outside water level and the smaller opening size acts as a barrier. Opposite behavior is observed for WP2 as high frequency nonlinear waves may be trapped inside the compartment due to obstruction at the opening and cause high values near the wall opposite to the opening. In case of filling level 2, wave elevations for both openings show a similar behavior except at some frequencies. This is expected since the free surface in filling level 2 is not directly open to the outer water surface as for filling level 1 (figure 40).

Figures 41 and 42 show non-dimensional added mass and damping coefficients in heave for opening 1 and 2 at filling levels 1 and 2, respectively. The added mass shows similar values for the two openings except near the first piston mode frequency. This may be because 3D effects are introduced due to the smaller opening. The damping shows similar behavior with slightly higher values for opening 2, mostly near the first piston mode resonance. Piston mode resonance is associated with large in/outflow through the opening and, therefore, for opening 2 we may have significant effect of vortex shedding from the appendage edges. The change in damping related with opening 2 is larger for filling level 1 since 3D effects due to flow separation at the opening edges will be higher for filling level 1.

5.3 Uncertainty and repeatability

Two sets of repetitions in addition to the main tests were performed to check for uncertainty and repeatability of the experiments. Repetition is not performed for all frequencies and cases because of the availability of lab resources. For filling level 1, 5 frequencies were chosen to cover the range from small to high frequencies along with some intermediate frequencies. Similarly, for filling level 2, 6 frequencies were selected. Figure 43 shows mean values with deviation for added mass and damping coefficients in heave and wave elevation amplitudes at filling level 1 and filling level 2. The results show acceptable deviation for all measured values. Deviation from mean values in added mass and damping is larger at smaller frequencies with the maximum deviation being 18% and 17%, respectively. Wave elevation values show larger deviation as compared to added mass and damping values at most frequencies but are within acceptable range. In particular, the maximum deviation is 23% and 20% for WP1 and WP2, respectively. Overall, the repeatability seems to be acceptable.

6 Conclusions

Experiments were performed in a wave flume on a thin walled prismatic hull form. The set-up was designed so to have nearly 2D flow conditions. The model has a damaged rectangular opening located on the side. Forced oscillatory heave tests in calm water have been carried out by varying the model-motion and damage opening parameters. Video recordings, measurements of wave elevation inside the damage compartment, and of the forces on the model were performed in all the experiments. Effect of filling depth, damage-opening length and air compressibility in airtight compartment were examined. Error sources in the tests discussed. Detailed investigation of the wave systems and resonance conditions of the floodwater was documented. The outcomes of the physical investigations can be summarized as follows:

- A simplified 2D single DoF (forced heave motions) damaged model is studied to identify resonance frequencies for piston and sloshing modes in a damaged ship section. Kong and Faltinsen [25] have demonstrated that they have an important effect on local floodwater behavior as well as on ship motions. We identify similar effects; sloshing and piston mode resonances are observed inside the damaged compartment. Non-dimensional added mass and damping coefficients in heave for intact and damaged sections at identical drafts are considerably different. Piston mode resonance causes a large effect on the added mass and damping coefficients.
- Results from forced heave tests demonstrate that filling depths can cause resonance frequencies to vary and wave systems associated with the examined filling levels can be quite different. These wave systems are associated with natural resonance frequencies of the floodwater inside the damaged compartment.
- A theoretical analysis is used to identify the linear natural frequencies for piston and sloshing modes. It helped in explaining the large change in added mass and the large peaks in damping and reasonable agreement is observed with the resonance occurrence in the model tests and with the related modeshapes from the experimental videos.
- At certain heave excitation frequencies, we obtained conditions that can lead to important local loads, e.g. secondary splash up as shown in figure 19.
- Air compressibility can have important effects. It slows down the flooding inside the damaged compartment, which is especially evident near piston mode resonance where almost no water enters

for an airtight damaged compartment. The sloshing mode remains unaffected as expected, this also verifies that near sloshing resonance exchange of floodwater through the opening is highly reduced.

- Since inflow/outflow of floodwater is highly limited for an airtight damaged compartment, the behavior is similar to a solid mass of water oscillating with the model, thus the added mass and damping in heave are similar to those of an intact section. However, air compressibility is associated with scaling issues and must be interpreted accordingly.
- Damage-opening length clearly influences the wave systems inside the damaged compartment. It does not show a considerable change in the hydrodynamic forces acting on the body. In this regard, the opening length/opening height effect should be investigated further.
- Repeatability of the tests can be viewed as acceptable.

The present experiments try to demonstrate the complex behavior of hull and floodwater interaction. A single DoF constrained model will not capture completely the complex physics of flooding and might amplify some dynamic effects. Present single DoF tests in heave are valuable in identifying important resonance phenomena. This experiment allowed investigating different relevant parameters of the problem and provides also a database for validation of numerical solutions, as shown in preliminary studies by Siddiqui et al. [36]. Freely floating coupled heave and roll tests to study the effect of the identified resonance frequencies represent our next research step.

7 Acknowledgement

The authors would like to acknowledge Trond Insett and Torgeir Wahl for their help with experimental setup in the flume. This work has been carried out at the Centre for Autonomous Marine Operations and Systems (AMOS). The Research Council of Norway (Norges Forskningsråd) is acknowledged as the main sponsor of AMOS. This work was supported by the Research Council of Norway through the Centre of Excellence funding scheme, Project number- 223254 AMOS.

8 References

1. Spouge, J. R., (1986). The technical investigation of the sin- king of the Ro-Ro ferry European gateway. Transactions of the Royal Institution of Naval Architects, 128: 49-72.
2. Spanos, D., and Papanikolaou, A., (2001) On the stability of fishing vessels with trapped water on deck. Ship Technology Research 48, 124–133.
3. Jasionowski, A., (2001). An integrated approach to damage ship survivability assessment. Ph.D. Thesis, University of Strathclyde.
4. Ruponen, P., (2007). Progressive flooding of a damaged passenger ship. PhD Thesis, Helsinki University of Technology.
5. Santos, T.A., and Guedes Soares, C., (2008). Study of damaged ship motions taking into account floodwater dynamics. Journal of Marine Science and Technology 13(3), 291-307.
6. Colicchio, G., Greco, M. and Faltinsen, O.M., (2006). A BEM-level set domain decomposition strategy for nonlinear and fragmented interfacial flows, International Journal for Numerical Methods in Engineering, 67/10.
7. Gao, Z., (2012). A hybrid approach to flooding and damaged ship dynamics. Ph.D. Thesis, University of Strathclyde.

8. Sadat-Hosseini, H., Kim, D-H., Carrica, P.M., Rhee, S.H., and Stern, F., (2016). URANS simulations for a flooded ship in calm water and regular beam waves. Ocean Engineering 120, 318-330.
9. Hashimoto, H., Kawamura, K., and Sueyoshi, M., (2017). A numerical simulation method for transient behavior of damaged ships associated with flooding. Ocean Engineering 143, 282-294.
10. Korkut, E., Altar, M. and Incecik, A., (2004). An experimental study of motion behavior with an intact and damaged Ro-Ro ship model. Ocean Engineering 31, 483-512.
11. Begovic, E., Mortola, G., Incecik, A., and Day, A.H., (2013). Experimental assessment of intact and damaged ship motions in head, beam and quartering seas. Ocean Engineering 72(1), 209–226.
12. Palazzi, L. and deKat, J., (2004). Model experiments and simulations of a damaged ship with air flow taken into account. Marine Technology 41(1), 38–44.
13. Ruponen, P., Kurvinen, P., Saisto, I. and Harras, J., (2013). Air compression in a flooded tank of a damaged ship. Ocean Engineering, 57, 64–71.
14. Khaddaj-Mallat, C., Alessandrini, B., Rousset, J.M. and Ferrant, P., (2012). An experimental study on the flooding of a damaged passenger ship. Ships and Offshore Structures, 7 (1), 55–71.
15. Lee S., You J, Lee H, Lim T, Rhee S.H., and Rhee K., (2012). Preliminary tests of a Damaged ship for CFD validation. International Journal of Naval Architecture and Ocean Engineering, 4,172-181.
16. Manderbacka, T., Ruponen, P., Kulovesi, J. and Matusiak, J.E., (2015). Model experiments of the transient response to flooding of the box shaped barge. Journal of Fluids and Structures, 57, 127-143.
17. Domeh, V.D.K., Sobey, A.J., and Hudson, D.A., (2015). A preliminary experimental investigation into the influence of compartment permeability on damaged ship response in waves. Applied Ocean Research, 52, 27–36.
18. Acanfora, M. and Luca, F.De., (2016). An experimental investigation into the influence of the damage openings on ship response. Applied Ocean Research, 58, 62–70.
19. Cichowicz, J., Vassalos, D. and Jasionowski, A., (2011). Experiments on a floating body subjected to Forced oscillation in Calm water at the presence of an open-to-sea compartment. Proceedings of the 12th International Ship Stability Workshop.
20. Smith T.W.P., Drake K.R., and Wrobel P (2009). Experiments on a damaged ship section, Analysis and Design of Marine Structures, CRC Press.
21. Vugts, Ir.J.H., (1968). The hydrodynamic coefficients for swaying, heaving and rolling cylinders in a free surface. Report 112S. Netherlands Ship Research Centre.
22. Faltinsen, O.M. and Timokha, A.N., (2009). Sloshing. Cambridge University Press.
23. Rognebakke, O.F., and Faltinsen, O.M., (2003). Coupling of sloshing and ship motions. Journal of Ship Research 47, no. 3, 208-221.
24. Kristiansen, T. and Faltinsen, O.M., (2010) A two-dimensional numerical and experimental study of resonant coupled ship and piston-mode motion. Applied Ocean Research. 32 (2), 158-176.
25. Kong, X.J. and Faltinsen, O.M., (2010). Piston mode and sloshing resonances in a damaged ship. The 29th International Conference on Ocean, Offshore and Arctic Engineering: Volume 3, Shanghai, China, June 6–11, 2010.
26. de Kat, J.O., (2000). Dynamics of a ship with a partially flooded compartment. Contemporary Ideas on Ship Stability: Elsevier Science Ltd.
27. Chang, B-C., (1999). On the damage survivability of Ro-Ro ships investigated by motion simulation in a seaway. Schiffstechnik-Ship Technology Research 46, 192–207.

28. Miles, J. and Munk, W. (1961). Harbor Paradox, Jour. Waterways and Harbors Div., Proc. ASCE, Vol 87, No WW3.
29. Molin, B. (2001). On the piston and sloshing modes in moonpools. Journal of Fluid Mechanics 430, 27-50.
30. Faltinsen, O.M., Rognebakke, O. and Timokha, A.N. (2007). Two-dimensional resonant piston-like sloshing in a moonpool. Journal of Fluid Mechanics 575, 359-397.
31. Newman, J.N., Sortland, B. and Vinje, T., (1984). Added mass and damping of rectangular bodies close to the free surface. Journal of Ship Research 28, no. 4, 219-225.
32. Ouellet, Y. and Datta, I., (1986). A survey of wave absorbers, Journal of Hydraulic Research, vol 24, 265 -279.
33. Olsen, H. and Johnsen, K., (1975). Nonlinear sloshing in rectangular tanks: a pilot study on the applicability of analytical models, Tech. Rep., Det Norske Veritas (DNV), Høvik, Norway, 74-72-5, Vol. 2.
34. Bouscasse, B., Antuono, M., Colagrossi, A., and Lugni, C., (2013). Numerical and Experimental Investigation of Nonlinear Shallow Water Sloshing. Int. J. Nonlinear Sci. Numer. Simul; 14(2), 123–138.
35. Malenica, S. and Zalar, M., (2000). An alternative method for linear hydrodynamics of air cushion supported floating bodies, The 15th International Workshop on Water Waves and Floating Bodies, 27 Feb-1 March, 2000.
36. Siddiqui, M.A., Greco, M., Colicchio, G., and Faltinsen, O.M., (2018). Validation of damaged ship hydrodynamics by a Domain Decomposition Approach using the Harmonic Polynomial Cell method and OpenFOAM, The 33rd International Workshop on Water Waves and Floating Bodies, April 4 to 7, 2018.

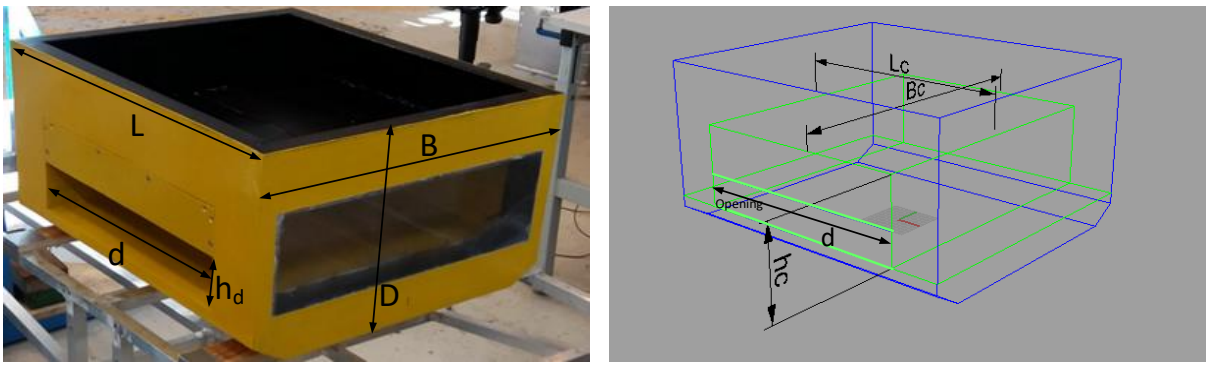

Fig 1. Definition of geometric variables in the three-dimensional view of the actual cross-section model (left) and definition of geometric variables for the internal compartment (right)

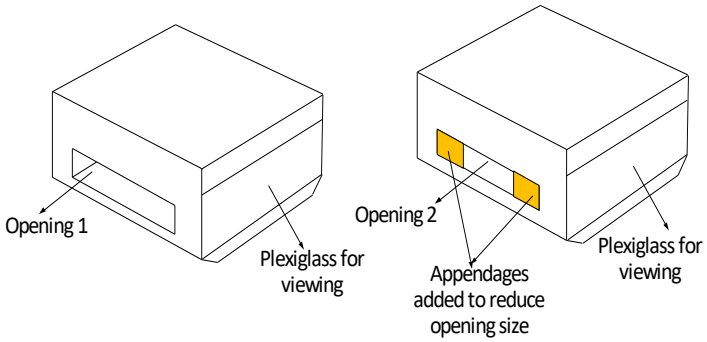

Fig 2. Sketch of the two damage openings studied in the tests

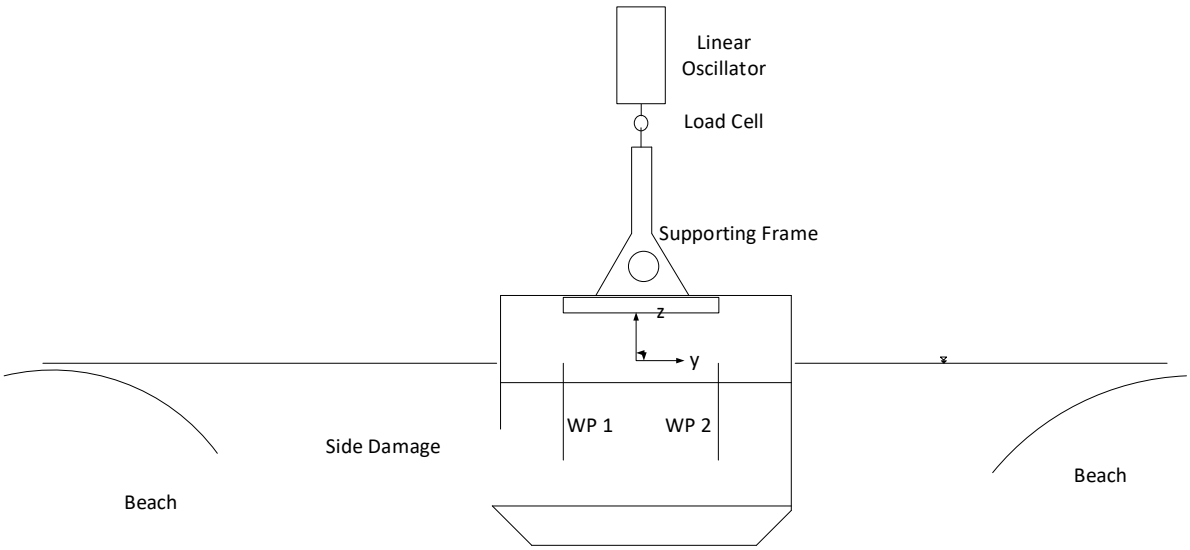

Fig 3. Sketch of the experimental setup (front view) for forced motion in heave

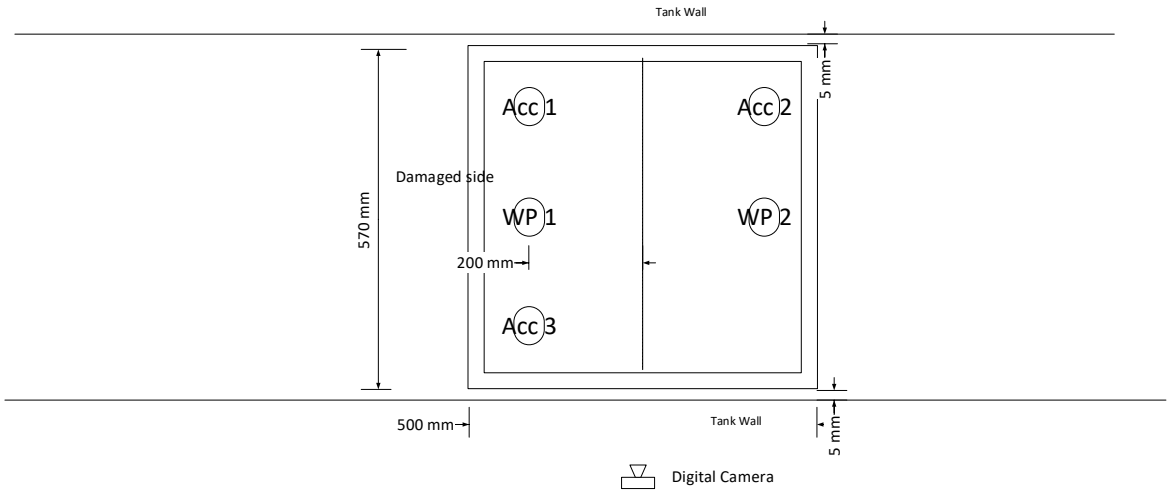

Fig 4. Sketch of the damaged section (top view) with location of wave probes (WP1-2) and accelerometers (Acc 1-3)

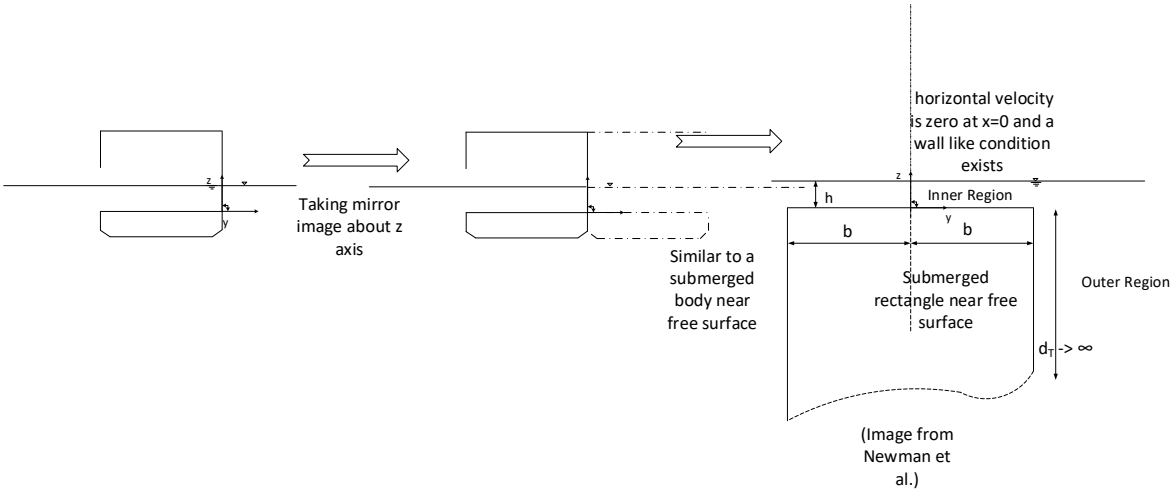

Fig 5. Simplification of forced heave motions for damaged section, using solution from Newman et al. [31]

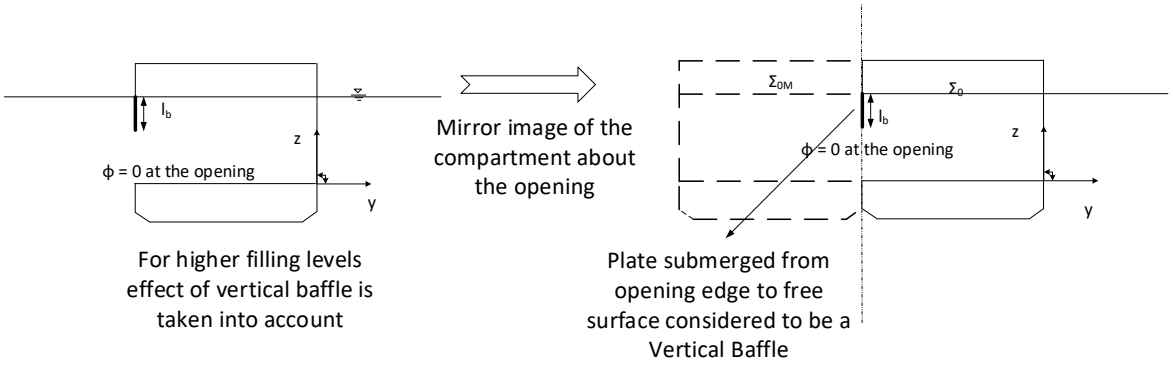

Fig 6. For filling level 2 and 3, effect of baffle at opening as shown in Faltinsen and Timokha [22] is used to calculate the modified natural frequencies

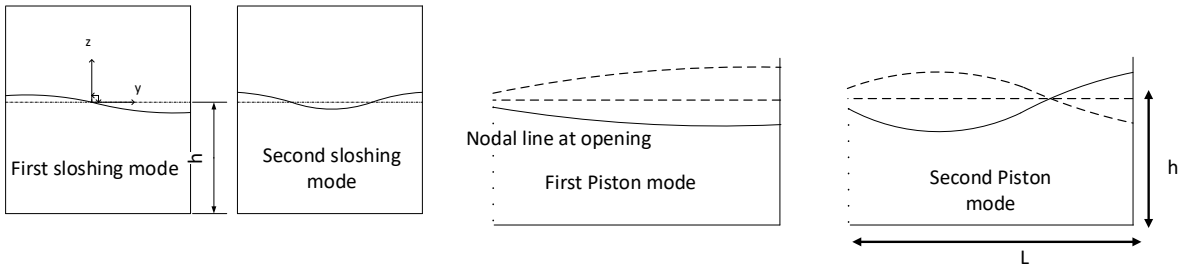

Fig 7. Sloshing natural modes (left) and natural piston modes calculated from Newman et al. [31] (right)

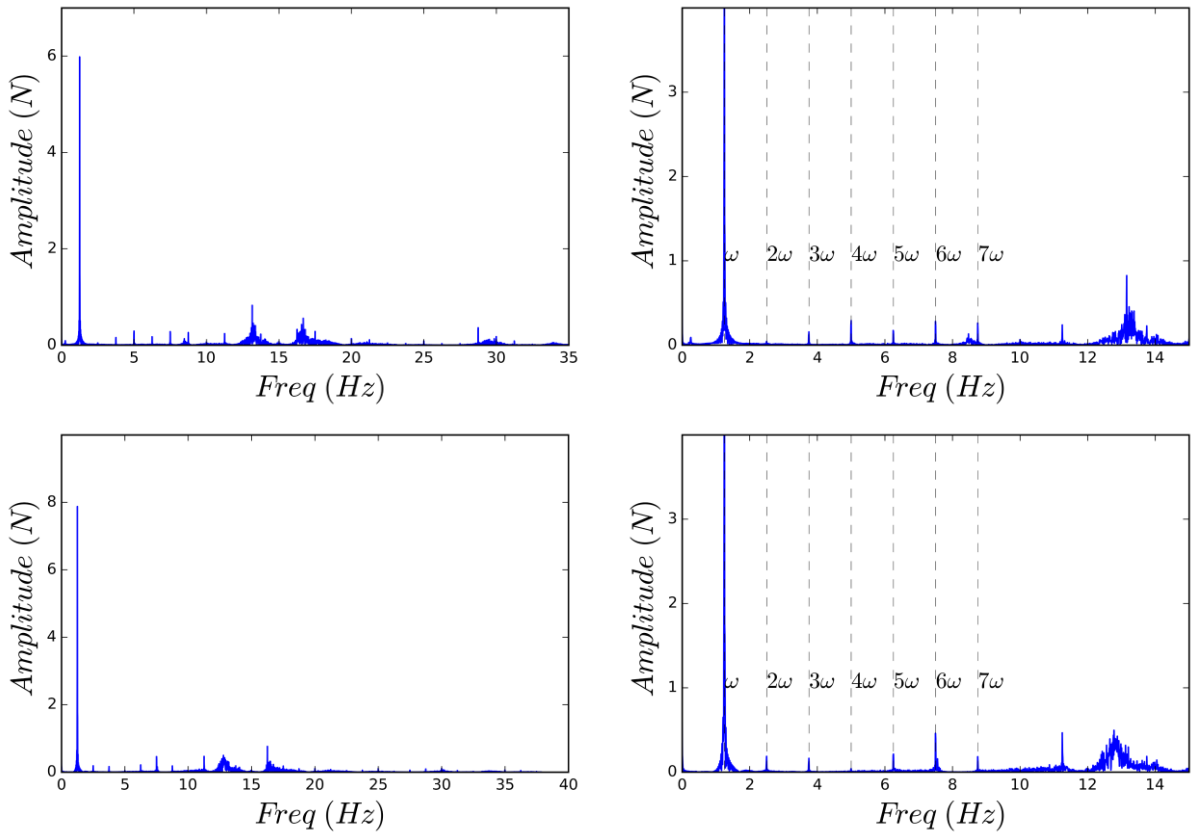

Fig 8. FFT analysis of force data for filling level 1(top left) and filling level 2 (bottom left) and forcing frequency $\omega = 1.25$, plots on the right show a magnified view of the FFT plots

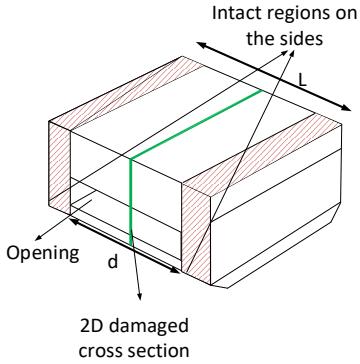

Fig 9. Illustration showing the calculation of added mass and damping for a 2D fully damaged section

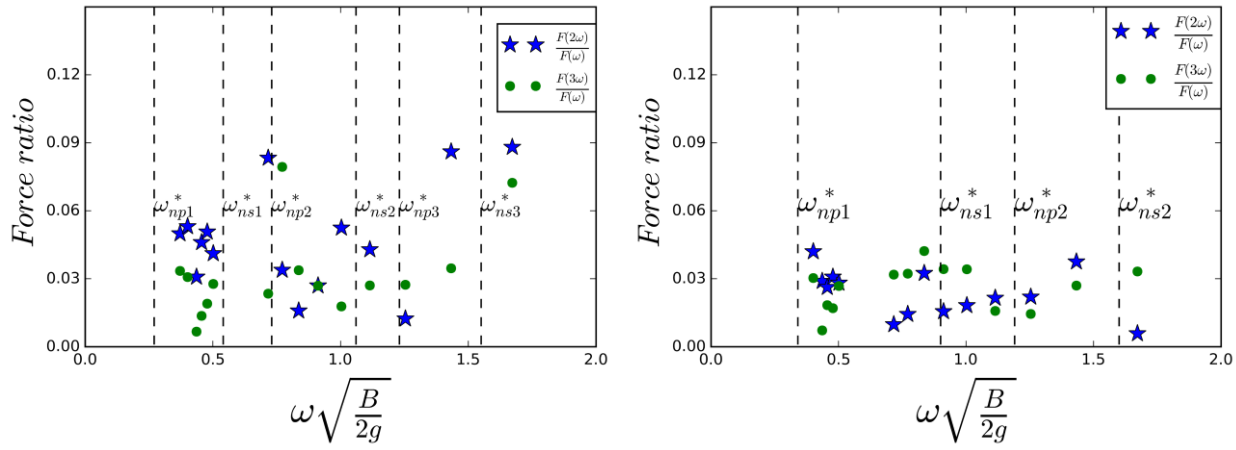

Fig 10. 2nd $F(2\omega)$ and 3rd $F(3\omega)$ order force amplitude components divided by force amplitude oscillating with forcing frequency for filling level 1 (left) and filling level 2 (right) and forcing amplitude $\eta_{3a} = 5\ mm$

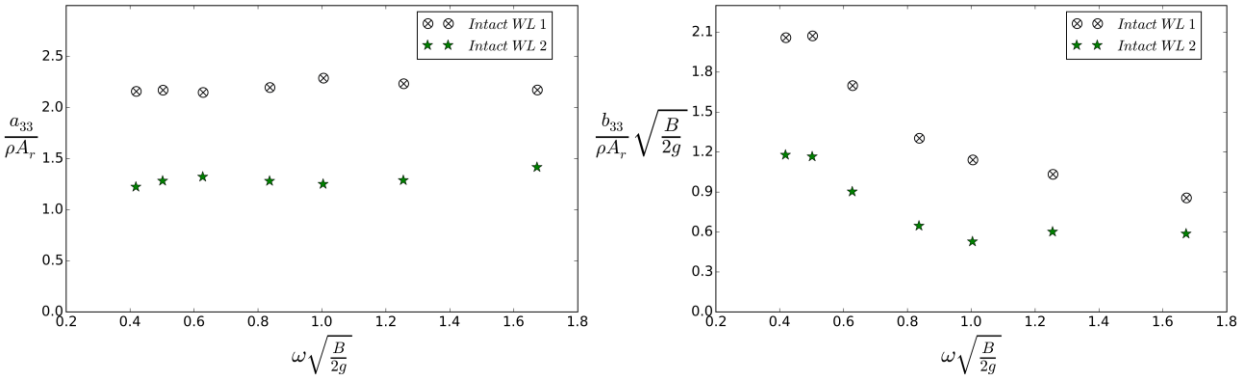

Fig 11. Added mass and damping coefficient in heave as a function of frequency for forced-heave motions of intact model in present experiments

Fig 12. Stationary model at three examined filling levels

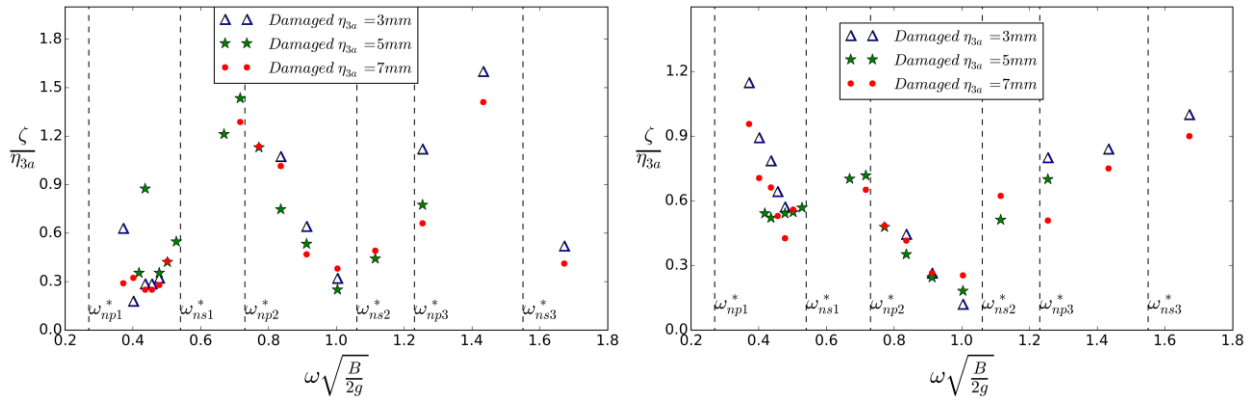

Fig 13. Wave probe RAOs at WP1 (left) & WP2 (right) inside damaged compartment as a function of non-dimensional frequency for three forced-heave amplitudes and filling level 1

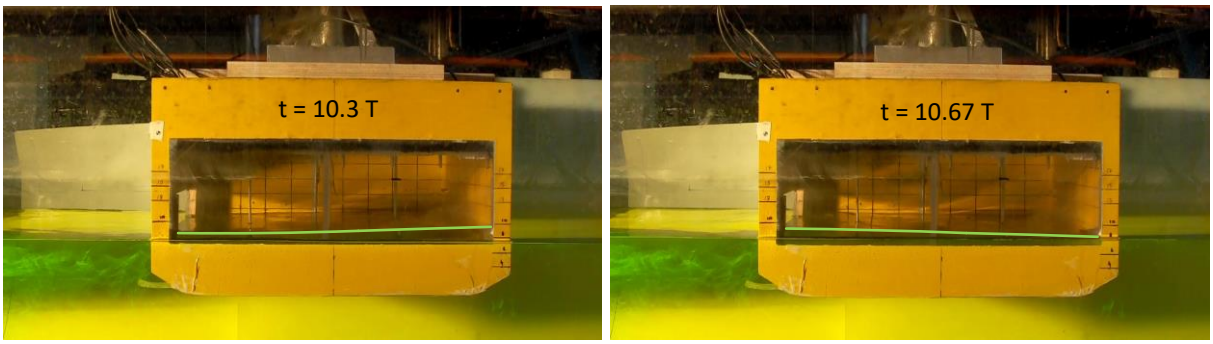

Fig 14. Scenario with standing waves at $\omega^* = 0.55$ and $\eta_{3a} = 5\ mm$ for filling level 1, similar to wave system I identified by Olsen and Johnson [33]

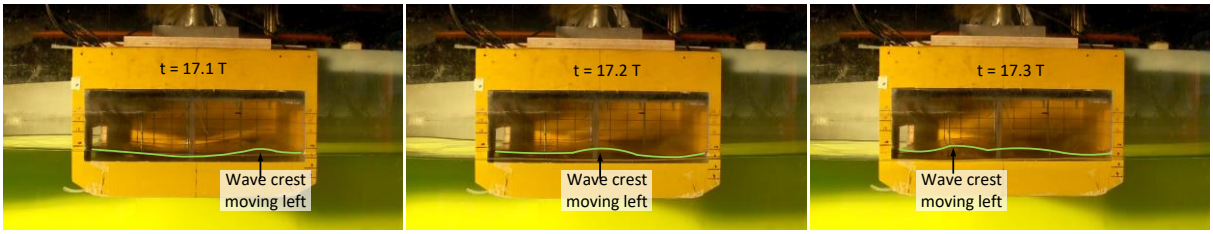

Fig 15. Progressive non-breaking waves at $\omega^* = 1$ and $\eta_{3a} = 5\ mm$ for filling level 1, similar to wave system II identified by Olsen and Johnson [33]

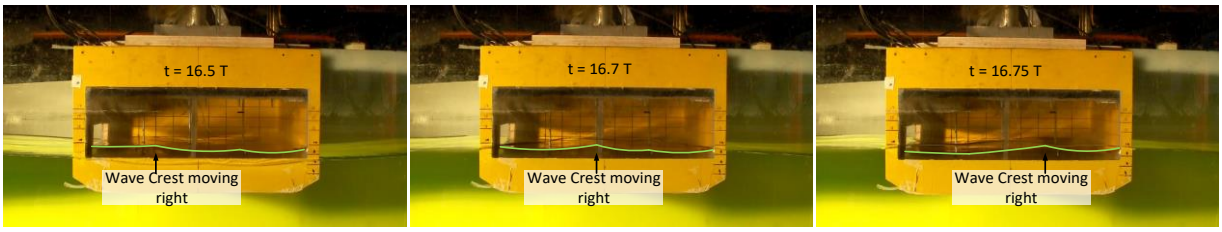

Fig 16. Progressive non-breaking waves at $\omega^* = 1.43$ and $\eta_{3a} = 5\ mm$ for filling level 1, similar to wave system II identified by Olsen and Johnson [33]

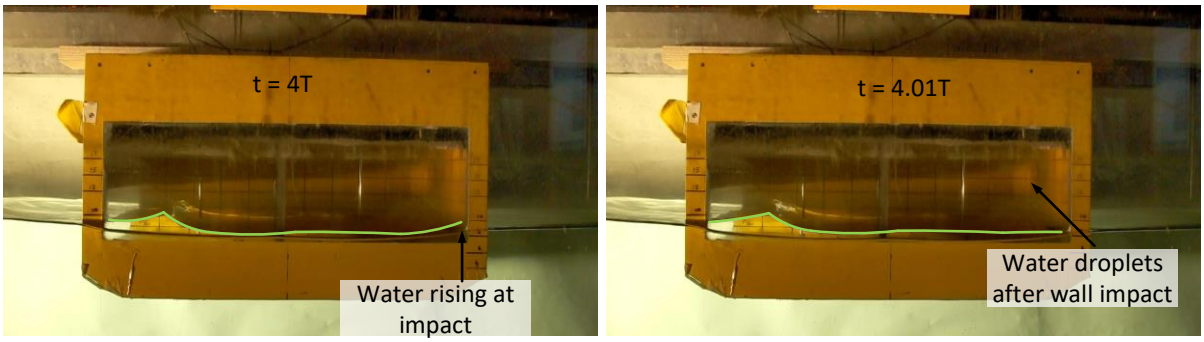

Fig 17. Progressive wave impacting the wall (left) with splash up leading to water spray (right) (not clear from the picture but visible in videos) for $\omega^* = 1.25$ and $\eta_{3a} = 5\ mm$ for filling level 1

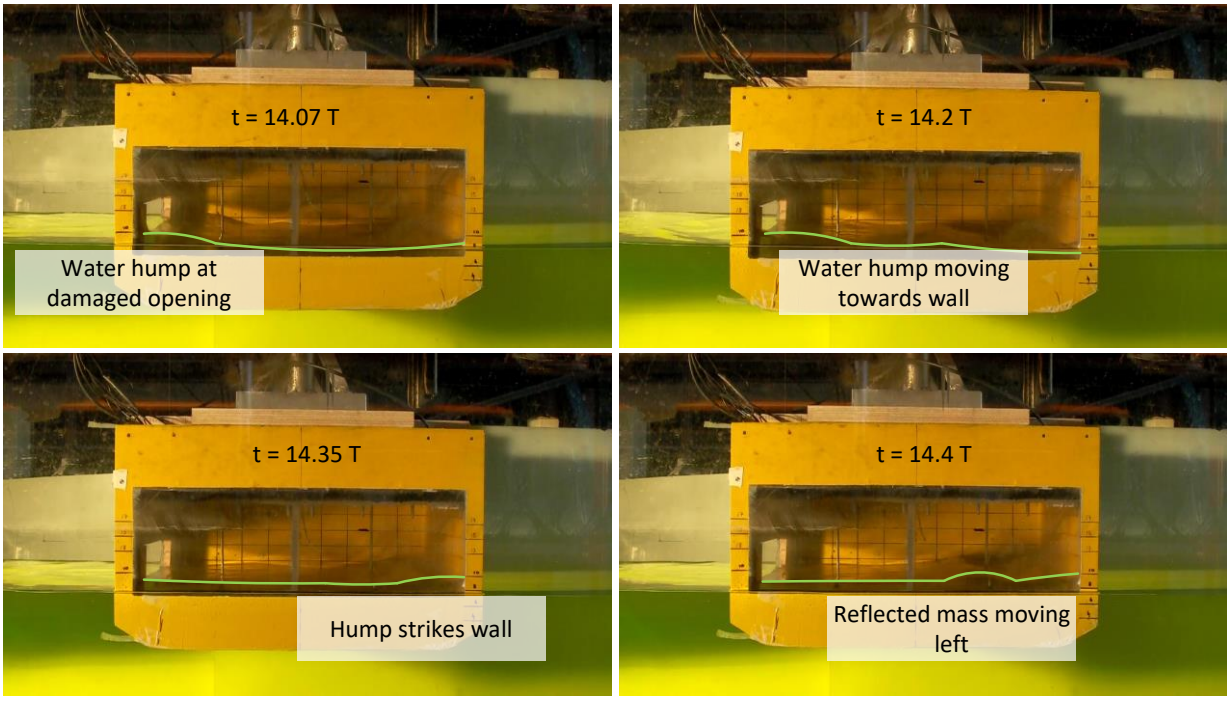

Fig 18. Second piston mode resonance at $\omega^* = 0.72$ and $\eta_{3a} = 5\ mm$ for filling level 1, similar to wave system IV identified by Olsen and Johnson [33]

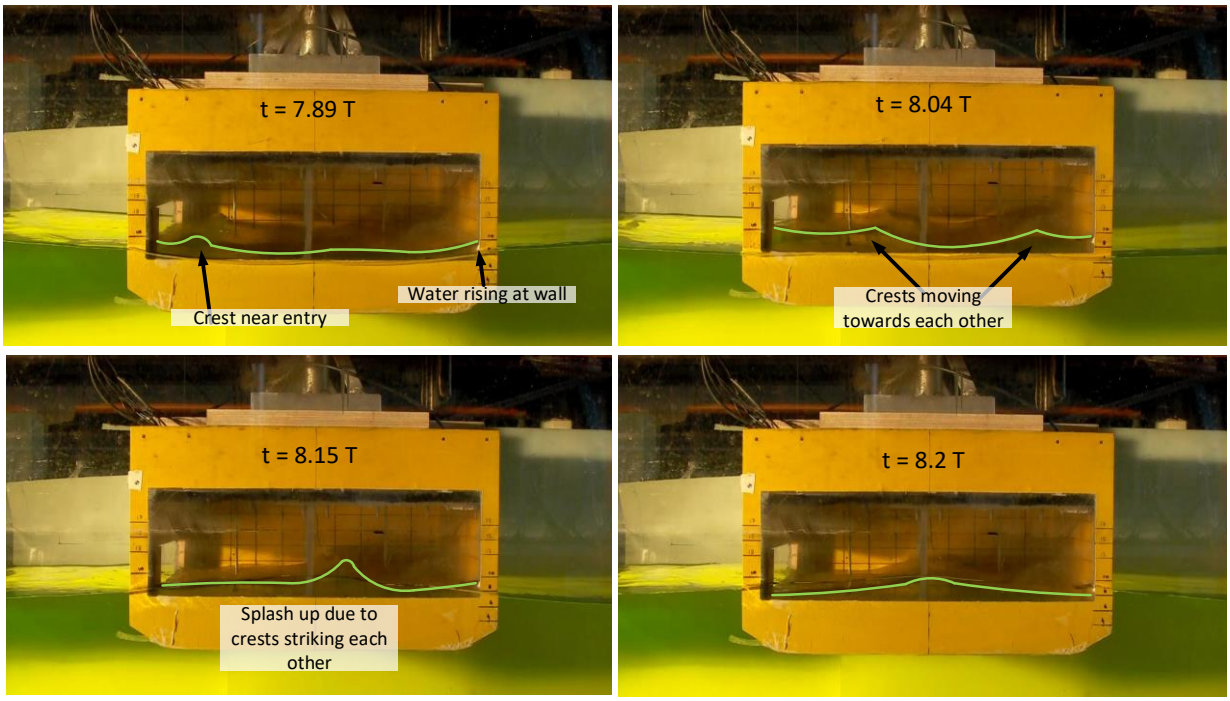

Fig 19. Secondary splash up in the middle of the tank at $\omega^* = 1.25$ and $\eta_{3a} = 7\ mm$ for filling level 1 identified for the first time by Bouscasse et al. [34]

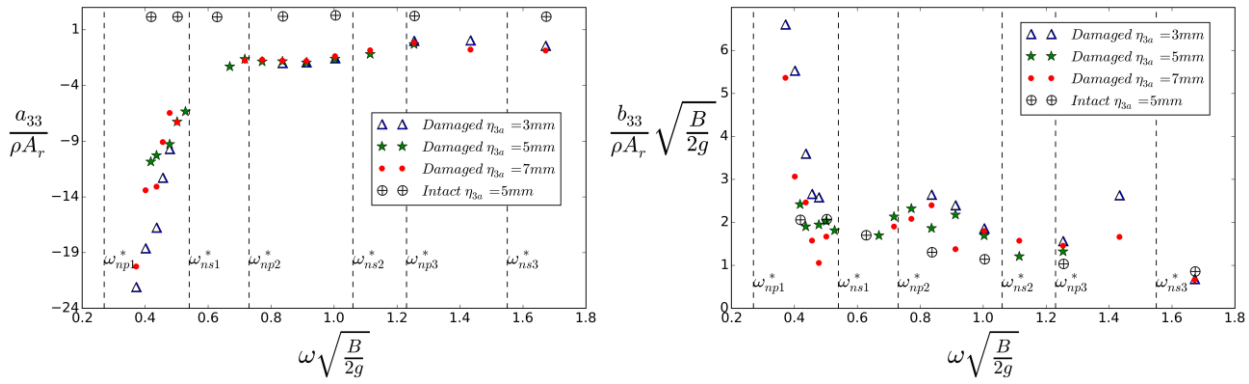

Fig 20. Added mass and damping coefficients in heave as a function of frequency for three forced-heave amplitudes and filling level 1

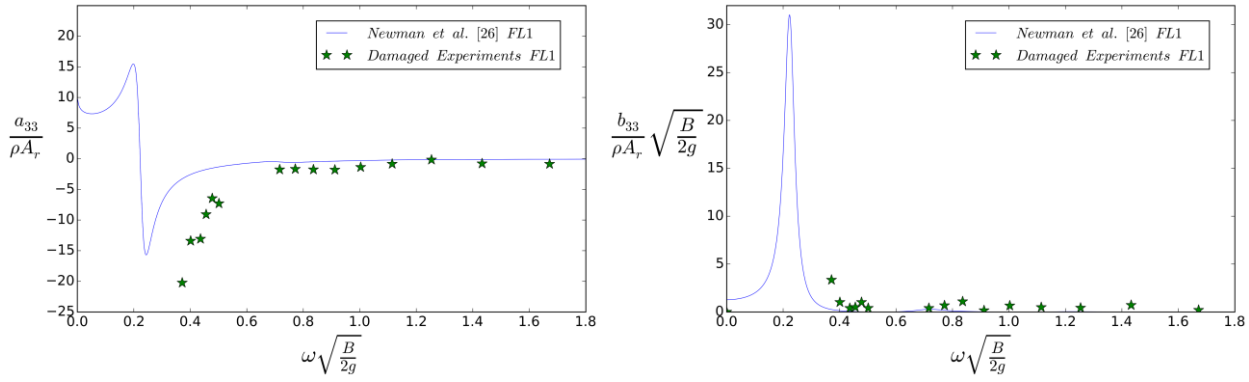

Fig 21. Added mass and damping coefficients in heave: comparison between experiments and Newman et al. [31] expression for filling level 1

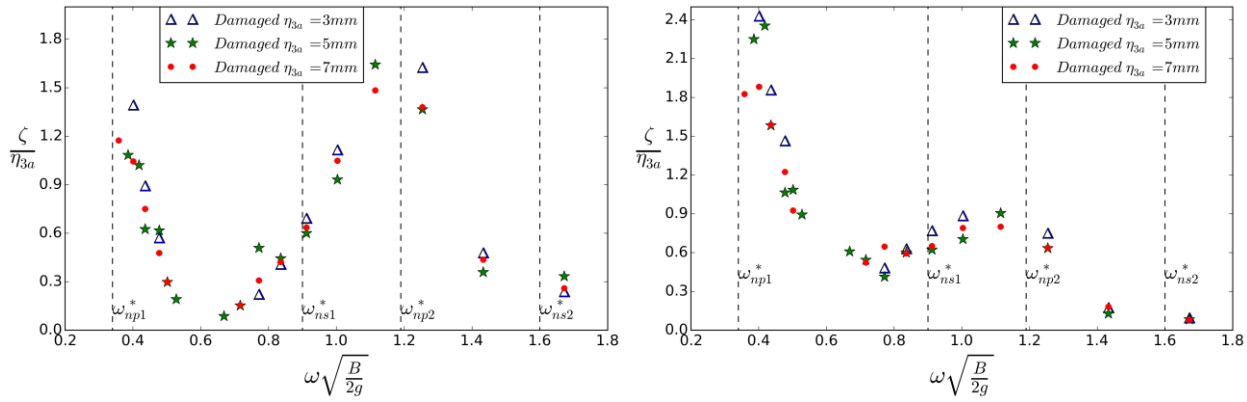

Fig 22. Wave probe RAOS at WP1 (left) & WP2 (right) inside damaged compartment as a function of frequency for three forced-heave amplitudes and filling level 2

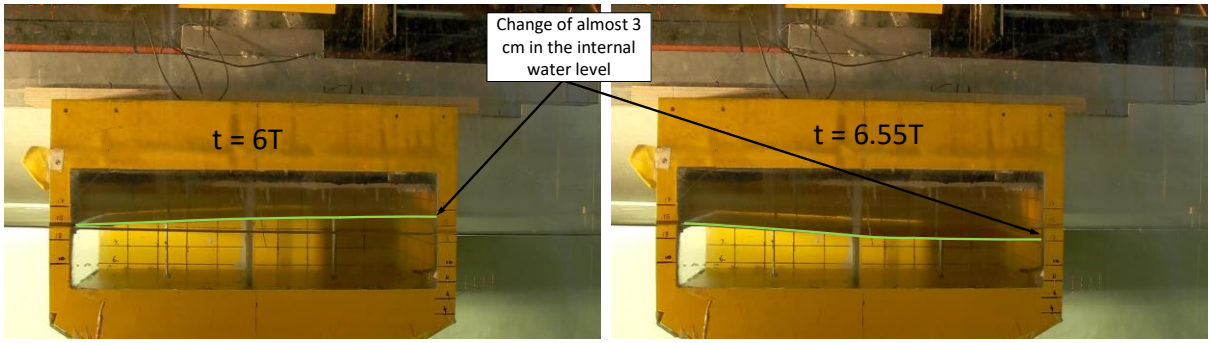

Fig 23. Piston mode resonance inside damaged compartment at $\omega^* = 0.41$ and $\eta_{3a} = 5\ mm$ for filling level 2

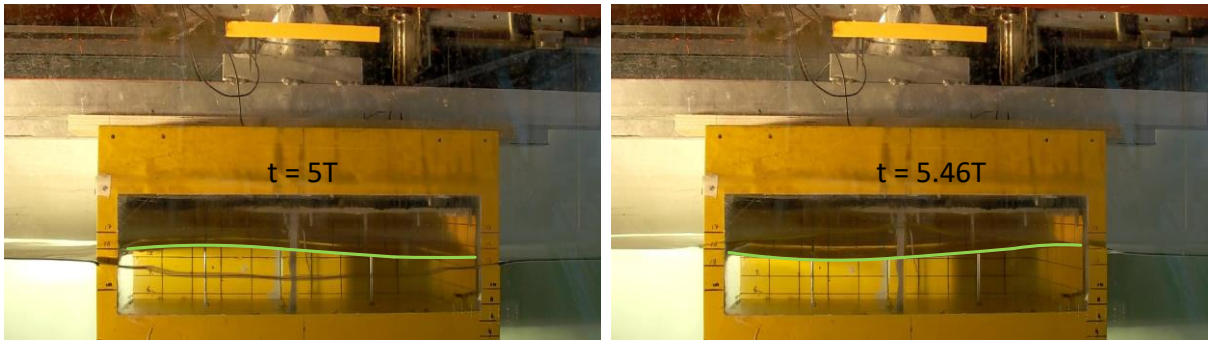

Fig 24. Second piston mode inside damaged compartment at $\omega^* = 1.25$ and $\eta_{3a} = 5\ mm$ for filling level 2

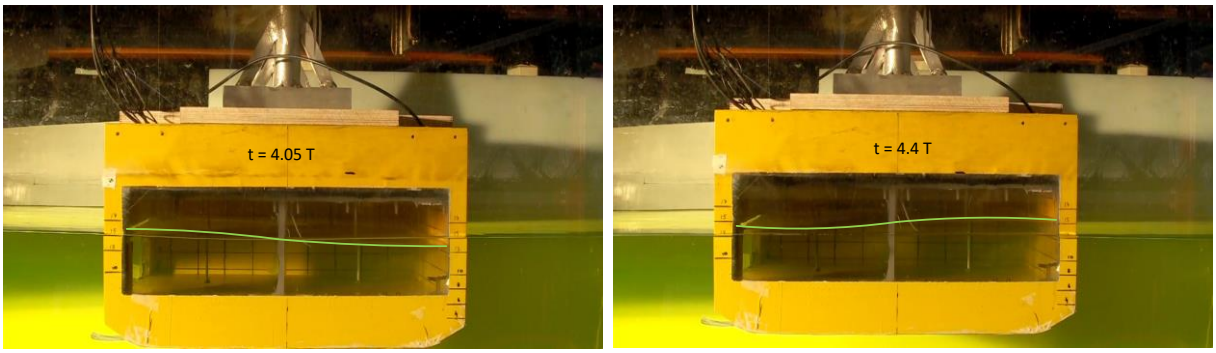

Fig 25. First natural sloshing mode inside damaged compartment at $\omega^* = 0.9$ and $\eta_{3a} = 5\ mm$ for filling level 2

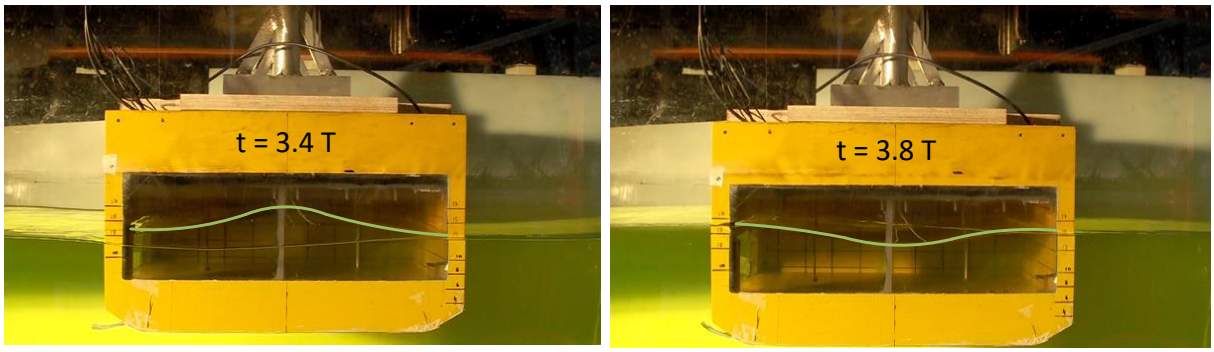

Fig 26. Second natural sloshing mode inside damaged compartment at $\omega^* = 1.67$ and $\eta_{3a} = 5\ mm$ for filling level 2

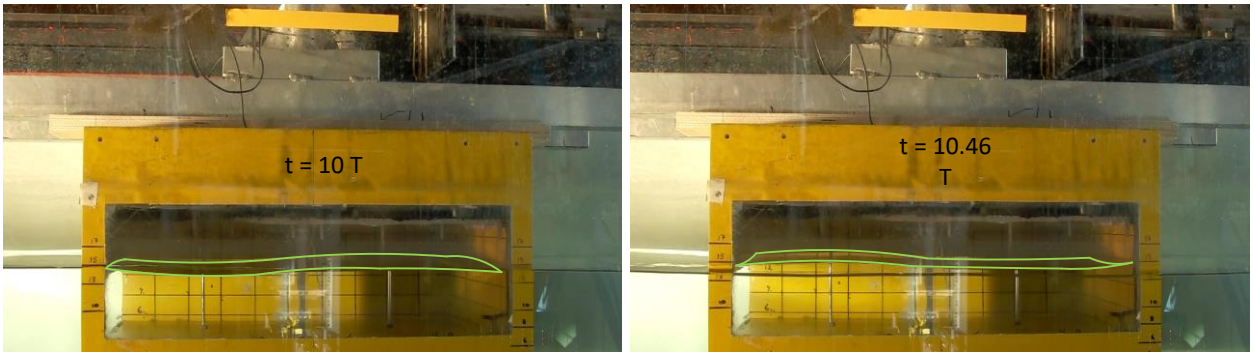

Fig 27. 3D sloshing mode inside damaged compartment at $\omega^* = 2$ and $\eta_{3a} = 5\ mm$ for filling level 2

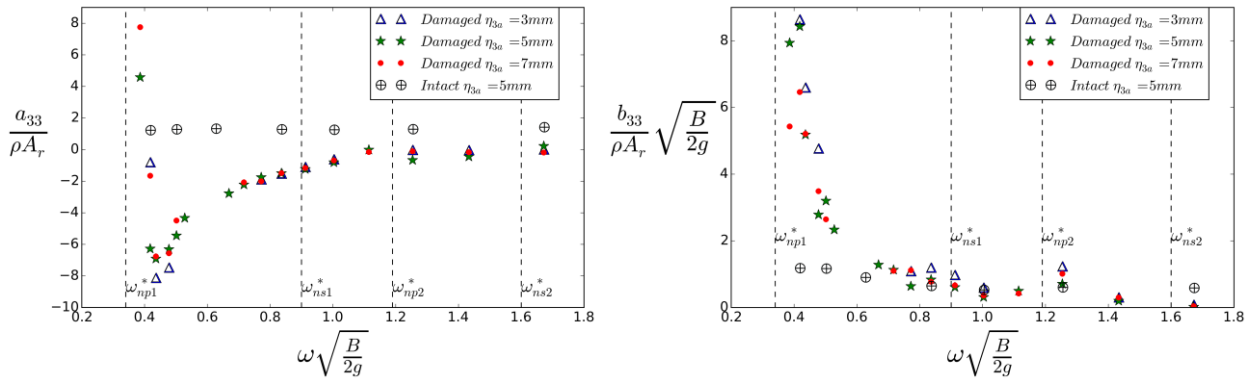

Fig 28. Added mass and damping coefficients in heave as a function of frequency for three forced-heave amplitudes and filling level 2

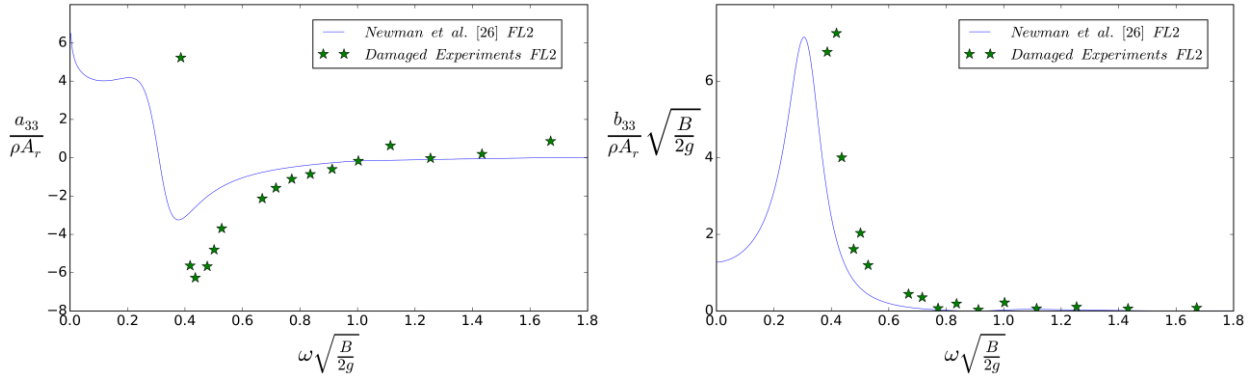

Fig 29. Added mass and damping coefficients in heave: comparison between experiments and Newman et al. [31] expression for filling level 2

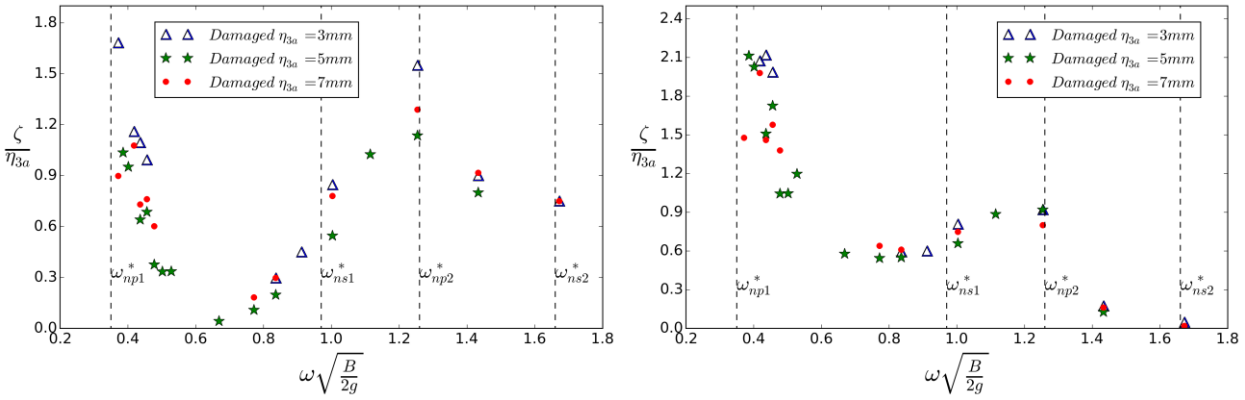

Fig 30. Wave probe RAOs at WP1 (left) & WP2 (right) inside damaged compartment as a function of frequency for three forced-heave amplitudes and filling level 3

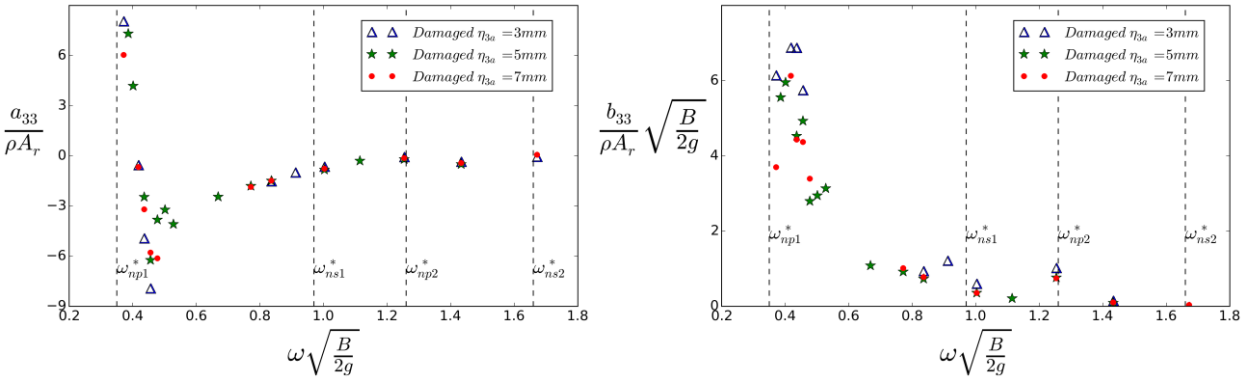

Fig 31. Added mass and damping coefficients in heave as a function of frequency for three forced-heave amplitudes and filling level 3

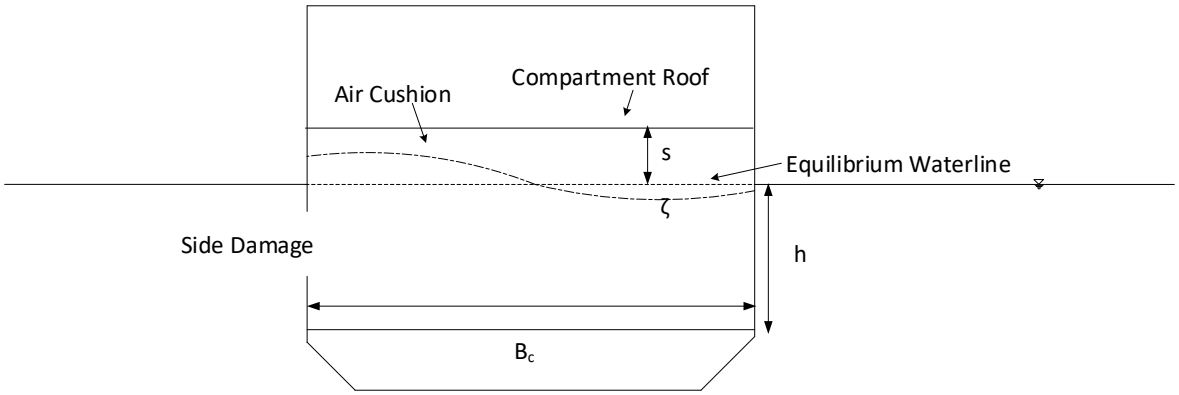

Figure 32. Sketch of compartment with air-cushion and related variables

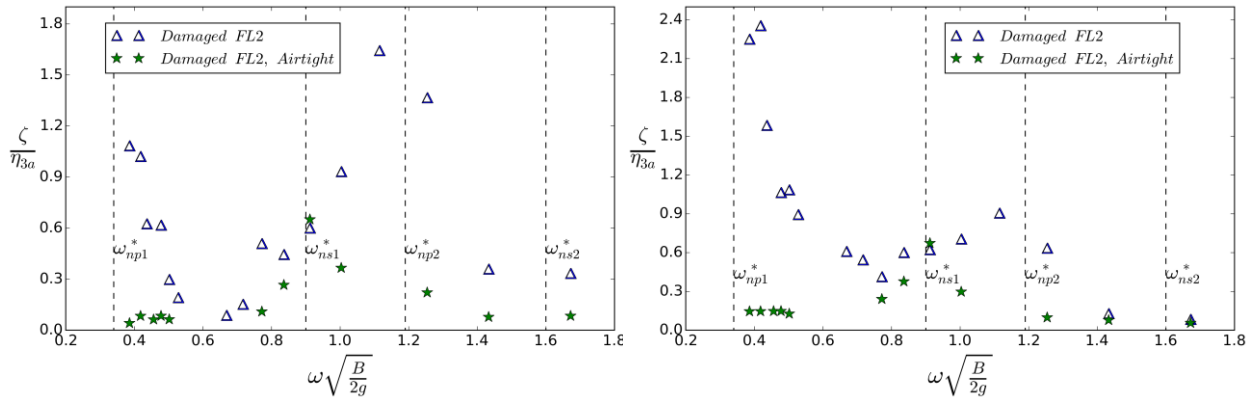

Fig 33. Wave probe RAOs WP1 (left) & WP2 (right) inside damaged compartment as a function of frequency, for ventilated and airtight conditions at filling level 2

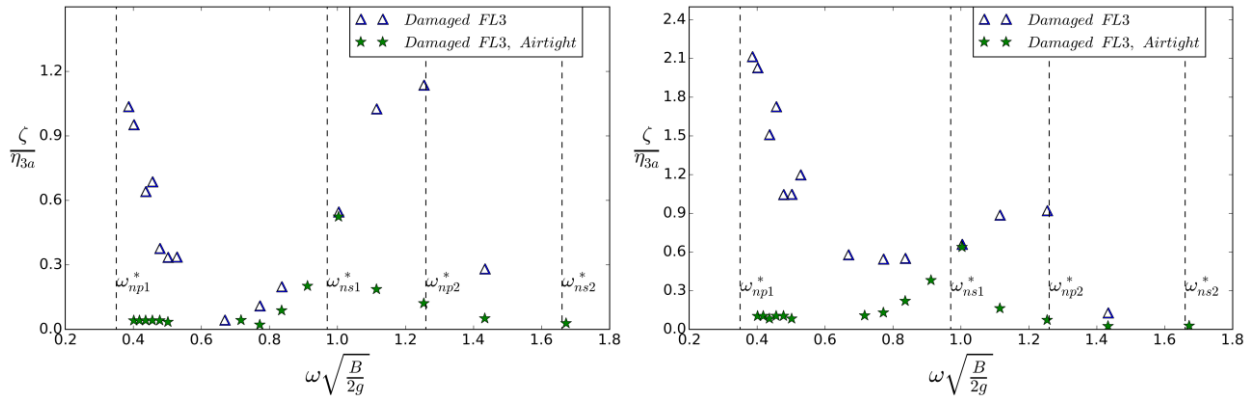

Fig 34. Wave probe RAOs WP1 (left) & WP2 (right) inside damaged compartment as a function of frequency, for ventilated and airtight conditions at filling level 3

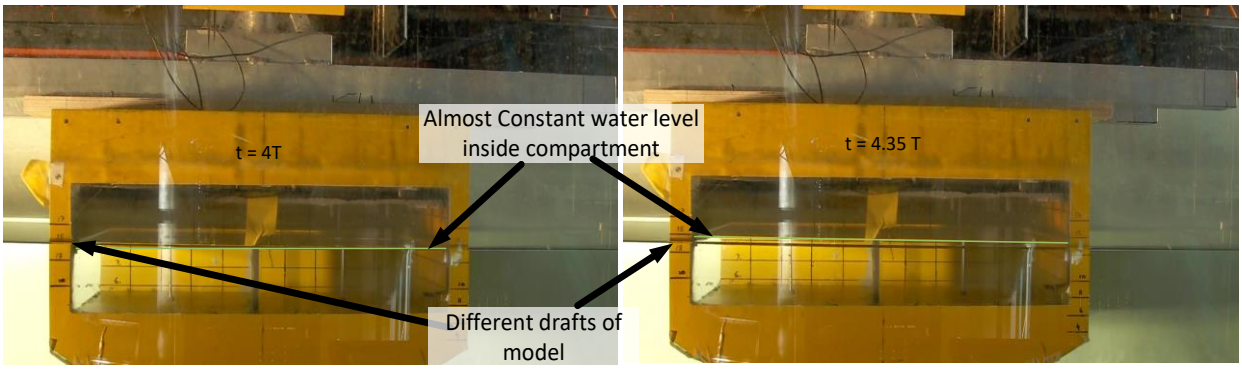

Fig 35. Water elevation (piston mode resonance absent) inside the airtight compartment for $\omega^* = 0.4$ and $\eta_{3a} = 5\ mm$ for filling level 2: the water level appears constant. Compare with figure 23 for the ventilated compartment in the same conditions.

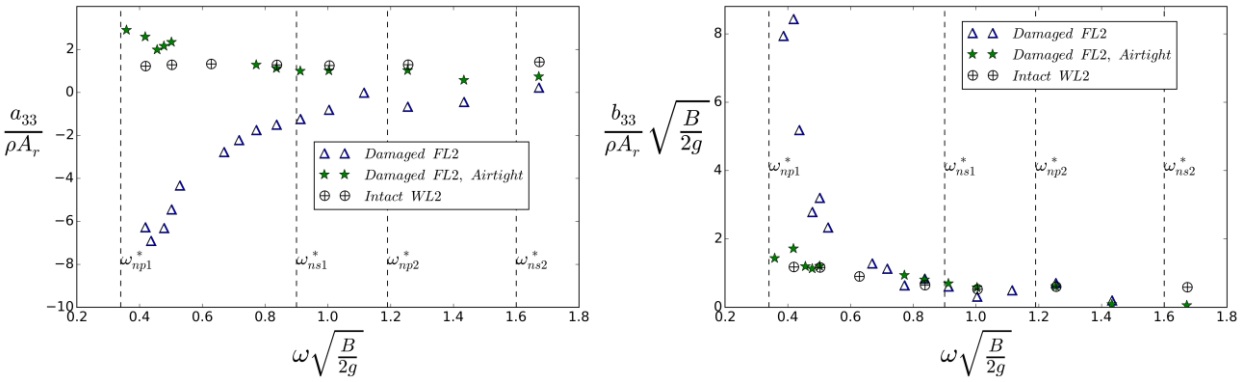

Fig 36. Added mass and damping coefficients in heave as a function of frequency, for ventilated and airtight conditions at filling level 2

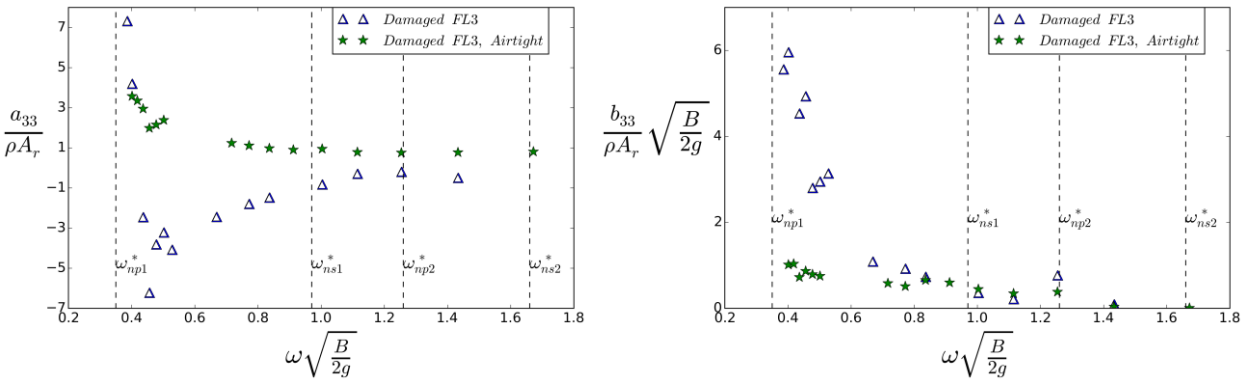

Fig 37. Added mass and damping coefficients in heave as a function of frequency, for ventilated and airtight conditions at filling level 3

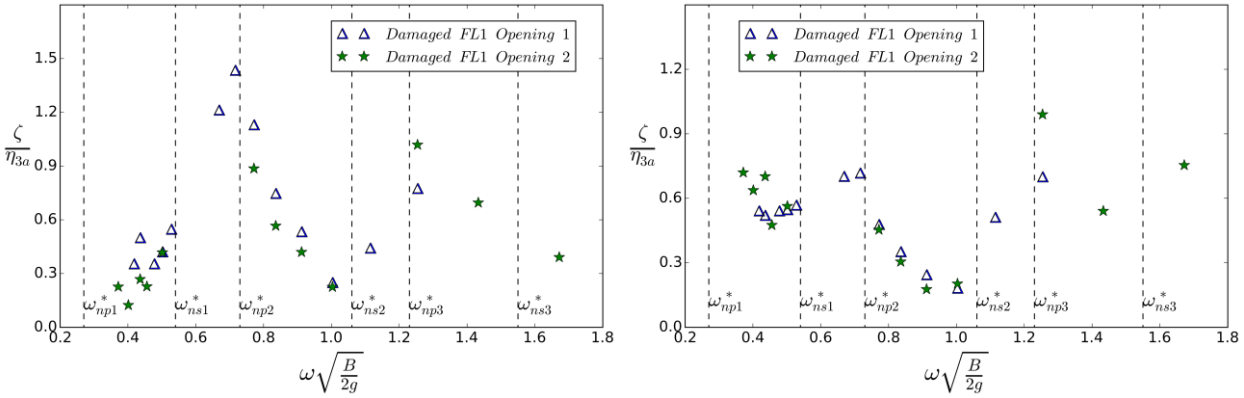

Fig 38. Wave probe RAOs at WP1 (left) & WP2 (right) inside damaged compartment as a function of frequency at $\eta_{3a} = 5\ mm$ for O1 and O2 at filling level 1

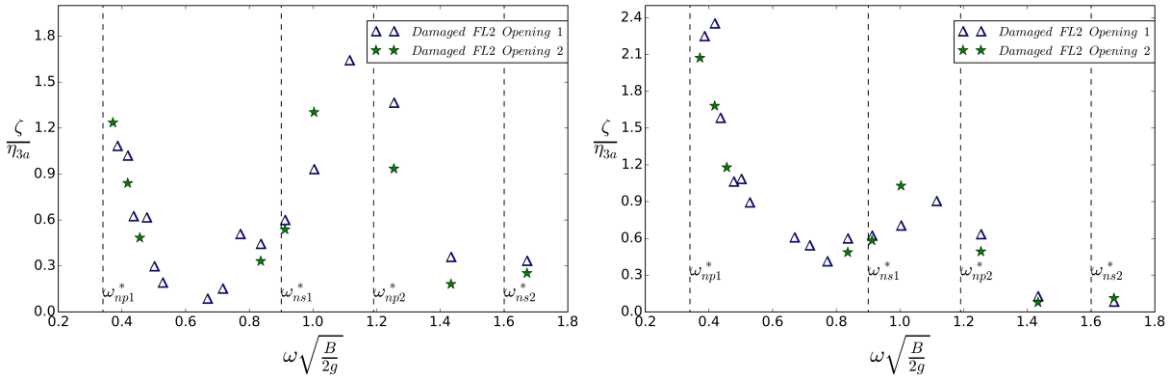

Fig 39. Wave probe RAOs at WP1 (left) & WP2 (right) inside damaged compartment as a function of frequency at $\eta_{3a} = 5\ mm$ for O1 and O2 at filling level 2

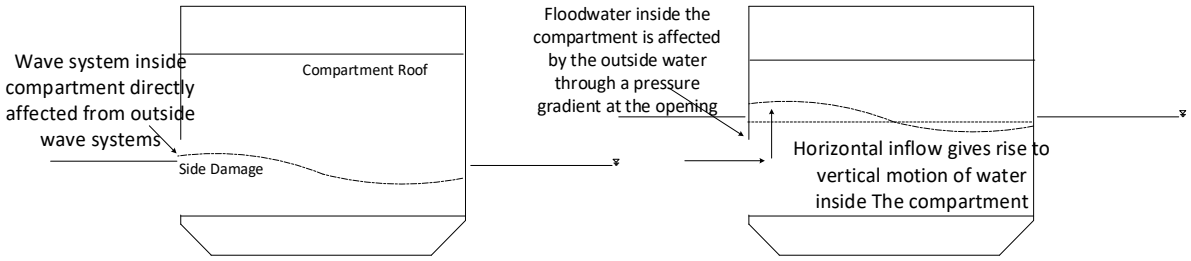

Fig 40. Effect of outside mean free surface on wave systems inside flooded compartment for filling level 1 (left) and filling level 2 and 3 (right)

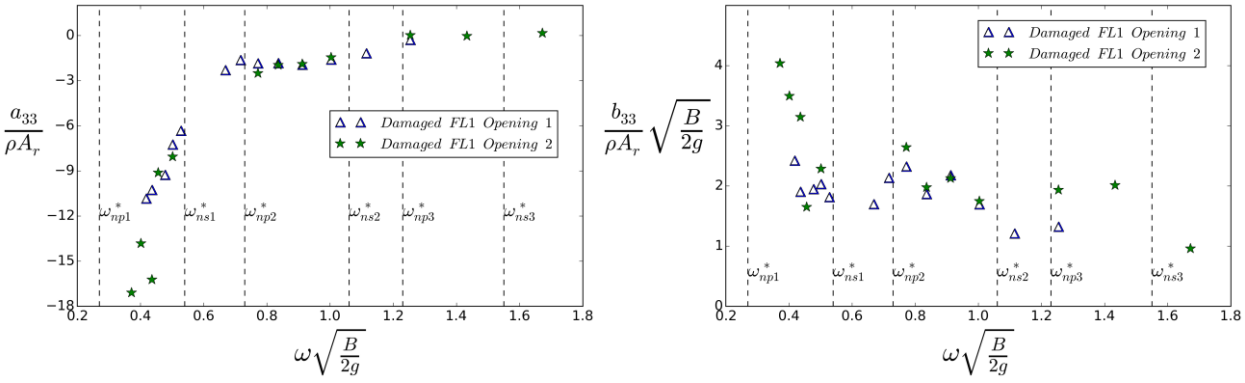

Fig 41. Added mass and damping coefficients in heave as a function of frequency at $\eta_{3a} = 5\ mm$ for O1 and O2 at filling level 1

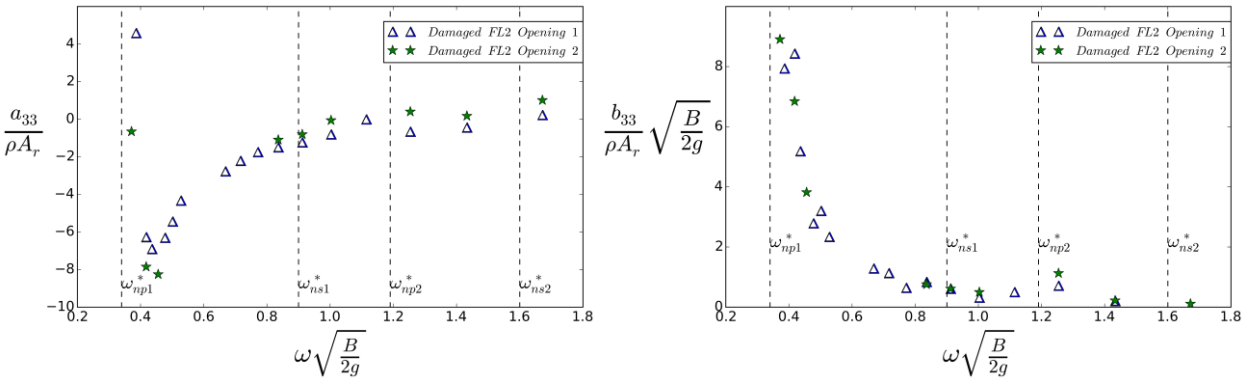

Fig 42. Added mass and damping coefficients in heave as a function of frequency at $\eta_{3a} = 5\ mm$ for O1 and O2 at filling level 2

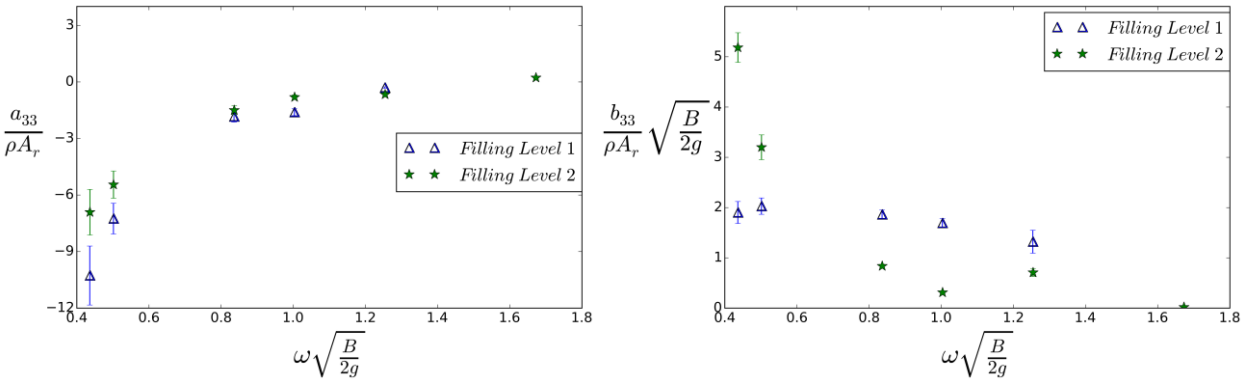

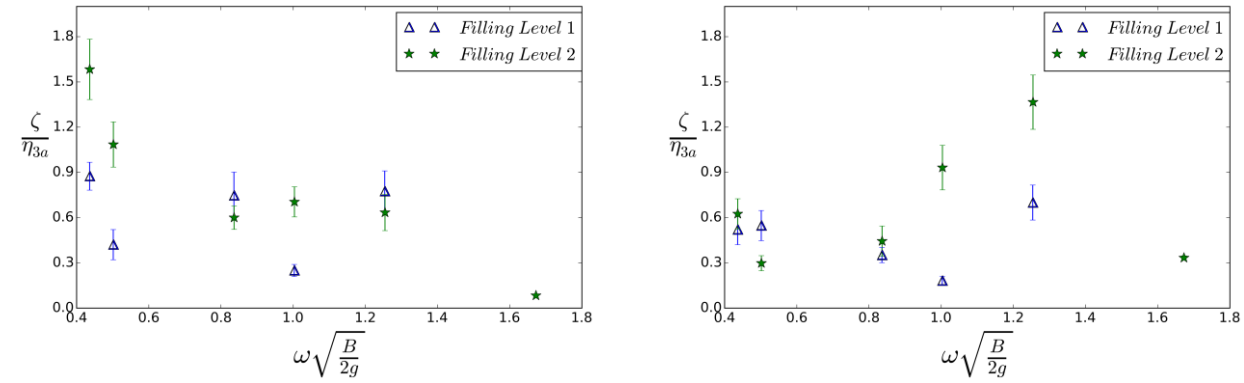

Fig 43. Deviation with mean values as a function of frequency in added mass, damping and wave elevation at $\eta_{3a} = 5\ mm$ and two filling levels

Table 1. Dimensions of the section model and compartment

Length (L)	0.57 m
Breadth (B)	0.505 m
Depth of model (D)	0.3 m
Side damage length (d)	0.4 m
Length of compartment (L_c)	0.4 m
Breadth of compartment (B_c)	0.5 m
Height of compartment (h_c)	0.15 m
Intended Scale	1:40

Table 2. Dimensions for the two openings

Openings	Side damage length d (m)	Height of damage opening h_d (m)
O1	0.4	0.08
O2	0.28	0.08

Table 3. Filling depth conditions and related parameters

	Condition	Water depth inside compartment h (cm)	Draft (cm)	Opening Condition	Equilibrium floodwater mass M_w (kg)
Waterline 1 (WL 1)	Intact	-	8	-	-
Waterline 2 (WL 2)	Intact	-	14	-	-
Filling Level 1 (FL1)	Damaged	3	8	Partially submerged	6
Filling Level 2 (FL2)	Damaged	9	14	Fully Submerged	18
Filling Level 3 (FL3)	Damaged	11	16	Fully Submerged	22

Table 4. Test matrix for forced heave motions

Filling levels (Draft (cm))	Forcing Amplitudes (mm)	Forcing period (s)	Condition
8	5	0.5 – 2.4	Intact
14	5	0.5 – 2.4	Intact
8	3,5,7	0.5 – 2.4	Damaged
14	3,5,7	0.5 – 2.4	Damaged
16	3,5,7	0.5 – 2.4	Damaged
14 (airtight)	5	0.5 – 2.4	Damaged
16 (airtight)	5	0.5 – 2.4	Damaged

Table 5. Relevant non-dimensional sloshing resonance frequencies $\omega_{nsj}\sqrt{\frac{B}{2g}}$, *j*=1,2,3 , for the examined damaged compartment at all filling levels (natural frequencies in bold are those within the range examined in the model tests)

Condition	h (m)	$\omega_{ns1}\sqrt{\frac{B}{2g}}$	$\omega_{ns2}\sqrt{\frac{B}{2g}}$	$\omega_{ns3}\sqrt{\frac{B}{2g}}$
Filling level 1	0.03	**0.54**	**1.06**	**1.55**
Filling level 2	0.09	**0.89**	**1.6**	2.09
Filling level 3	0.11	**0.97**	**1.66**	2.14

Table 6. Relevant non-dimensional piston mode frequencies $\omega_{npj}\sqrt{\frac{B}{2g}}$, *j*=1,2,3, for the examined damaged compartment at all filling levels (natural frequencies in bold are those within the range examined in the model tests)

Condition	h (m)	l_b (m)	$\omega_{np1}\sqrt{\frac{B}{2g}}$	$\omega_{np1}'\sqrt{\frac{B}{2g}}$	$\omega_{np2}\sqrt{\frac{B}{2g}}$	$\omega_{np2}'\sqrt{\frac{B}{2g}}$	$\omega_{np3}\sqrt{\frac{B}{2g}}$	$\omega_{np3}'\sqrt{\frac{B}{2g}}$
Filling level 1	0.03	0	0.27	0.27	**0.73**	**0.73**	**1.23**	**1.23**
Filling level 2	0.09	0.01	**0.3424**	**0.3418**	**1.1809**	**1.1784**	1.874	1.8688
Filling level 3	0.11	0.03	**0.3611**	**0.3564**	**1.282**	**1.2605**	1.9768	1.9276

Table 7. Error/uncertainty for the instruments used in current experiments

Instrument	Error/uncertainty	Unit
Dynamometer	0.75-1	N
Wave Probes	0.001-0.002	m
Accelerometers	0.05-0.1	m/s^2